

**Spatial filtering
and automatic alignment
of a high power CPA laser system**

Henrik Andersson

Diploma Paper
Lund Reports on Atomic Physics, LRAP 343
Lund, June 2005

Abstract

Spatial filtering is a crucial part of all large high power laser systems to prevent laser induced damage in optical components. In this report design considerations for the spatial filter used at the Lund Terawatt Laser, and an automatic alignment system that aligns the spatial filter is presented. The laser system considered is a 30 TW chirped pulse amplification (CPA) system with a titanium sapphire oscillator. The spatial filter is designed to remove the unwanted laser modes with divergence above $\pm 200 \mu\text{rad}$. The filter is placed before the final amplifier where the pulses are about 260 ps in duration and have pulse energies up to 500 mJ. Thermal variations induce a drift of the beam in the laser system, and hence an automatic alignment of the spatial filter is crucial for its functionality. Such an alignment system is presented in this report as well as the spatial filter.

Sammanfattning

Spatialfiltrering är en viktig del av hög-effekts lasersystem för att förhindra skador på komponenter i laserstrålens väg. I denna rapport diskuteras designen för spatialfiltret i terawatt lasern vid Lunds universitet. Lasern har en topp effekt på 30 TW och förstärkningen bygger på chirped pulse amplification (CPA) med en titansafir oscillator. Spatialfiltret är designat att ta bort icke önskade lasermoder med divergens över $\pm 200 \mu\text{rad}$. Filtret är placerat före sista förstärkaren där pulserna är ca. 260 ps långa och pulsenergi på 500 mJ. Termiska variationer medför en drift av laserstrålen i systemet och därför är ett automatiskt linjeringssystem nödvändigt för spatialfiltrets funktion. Ett sådant linjeringssystem har byggts och beskrivs i rapporten.

Contents

1	Introduction	5
1.1	The Lund multi-terawatt laser system	6
1.2	Chirped pulse amplification	7
2	The spatial filter	9
2.1	Theoretical analysis of a laser beam propagating through a spatial filter	10
2.2	Problems with the old spatial filter	13
2.3	Problems induced with spatial filtering	14
2.3.1	Dispersion	14
2.3.2	Back-scattered light	16
2.4	Pinhole	16
2.4.1	Formation of plasma	17
2.4.2	Plasma closure	18
2.4.3	Geometrical designs and material of the pinhole	19
2.5	Vacuum chamber	24
3	Automatic alignment	26
3.1	Beam drift	27
3.1.1	Shot to shot variations in the beam	27
3.2	Choice of fixed points in the laser system	29
3.3	The detection system	30
3.3.1	Detection of the beam	31
3.4	The control system	33
3.4.1	Piezoelectric crystals	33
3.4.2	Data processing	34
4	Results and discussion	37
4.1	The spatial filter	37
4.1.1	Future work on spatial filtering	40
4.2	Automatic alignment	41

4.2.1	Future work on automatic alignment	41
5	Conclusions	45
6	Acknowledgements	46
	Bibliography	47
A	The Beam Control program	49
A.1	Main VI, 'Beam Control.vi'	49
A.1.1	SubVI:s	53
A.1.2	Other VI:s	56
B	Camera	57

Chapter 1

Introduction

Spatial filters are used in many types of laser systems to remove high frequency spatial components in the laser beam. In high-energy systems a smooth intensity distribution across the beam is desired because intensity peaks (hotspots) might cause damage to components such as amplifying crystals or gratings. For such systems high spatial frequencies are removed in spatial filters. Which frequencies to remove is a compromise of energy loss and mode quality. For the system considered in this report one of the main purposes of the spatial filter is to prevent any hot spots from reaching the final amplifier (on optical table 3, see Figure 1.1). In this spatial filter frequencies with divergence (the larger frequency the larger the divergence) above $\pm 200 \mu\text{rad}$ are removed. A small focal spot is often also desirable which is achieved with spatial filtering.

The terawatt laser at Lund High Power Laser Facility was built in 1992. Modifications to improve this laser have been made continuously since then. Those modifications have improved beam quality and increased the peak power in the system. This project is yet another step in this continuous process to upgrade the system. The aim of the project was to increase the quality of the spatial filtering. This laser beam has previously been filtered but due to increasing demands for higher beam quality it was decided to make this improvement.

A system for controlling the beam direction was also built, during the project, to stabilize the laser beam and to make the spatial filter work at its optimum. Previously there has been a drift during the day due to temperature variations in the room and different laser components. This drift is now compensated for.

The outline of this report is as follows. In the rest of this chapter a brief description of the terawatt laser and chirped pulse amplification (CPA) is presented. In Chapter 2 spatial filtering and the design of a refractive

spatial filter is discussed. In Chapter 3 the previous problems with beam drift and the automatic alignment system, to compensate for this, is described. Finally, in Chapter 4 all results are presented and discussed, including a brief discussion of further possible improvements of the laser system concerning issues reported in this report.

1.1 The Lund multi-terawatt laser system

The system is based on the CPA technique, described below, with a titanium sapphire oscillator delivering pulses with a centre wavelength of 800 nm and a bandwidth of 25 nm. The pulse duration is below 35 fs (FWHM) and with a pulse energy of 1.1 J resulting in a peak power of 30 TW.

The pulse repetition frequency of the system is 10 Hz and the size of the focused beam is less than 1.3 times the diffraction limit. An outline of the whole laser system can be seen in figure 1.1.

The recently performed modifications presented in this report concerns the first multi-pass amplifier and the spatial filter, see Figure 1.2 for a schematic view of this part of the system. Today the system serves two separate experimental areas. The beam is split in two (beam splitter marked as BS in figure 1.2) most of the beam (75%) is directed to one of the experimental areas and the remaining part is further amplified before it is sent into the second experimental area. Pulse energies at the two experimental areas are 150 mJ and 1.1 J, respectively.

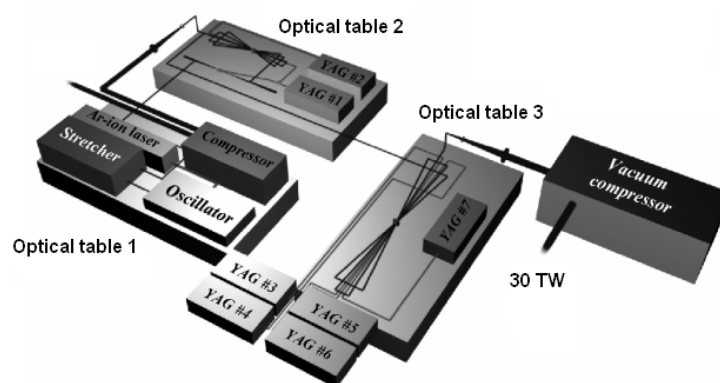


Figure 1.1: Schematic picture of the 10 Hz terawatt laser system in Lund

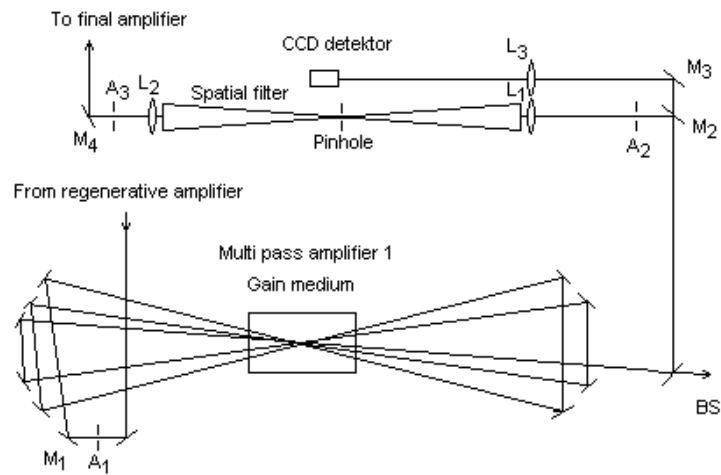


Figure 1.2: A schematic picture of the first multi-pass amplifier and the spatial filter

1.2 Chirped pulse amplification

Chirped pulse amplification is a relatively new technique and has been developed in the last couple of decades. The basic principle of CPA is to create a short pulse and then stretch it, amplify it and recompress it to its original pulse width. See figure 1.3 for a schematic picture of the process. First extremely short pulses, of the order of femtoseconds, are generated in an oscillator. This is achieved with mode-locking, which means that only those laser modes that will contribute to a short pulse (a wide band of frequencies is required to build up a short pulse) will receive positive gain in the amplifying crystal. In a titanium sapphire oscillator the mode locking is achieved with a nonlinear effect (optical Kerr effect) in the crystal which focuses light at high intensities. The pulses generated in the oscillator are stretched in time to decrease its power which otherwise would damage optical components. In the pulse stretcher a dispersion of the beam is introduced. This dispersion can be introduced by gratings or prisms. The pulses are then amplified in several stages. Only a fraction of the oscillator pulses are amplified. The repetition rate in the oscillator is in the order of 100 MHz while the amplified pulse repetition rate is significantly less (10 Hz for the system described in this report). The stretched and amplified pulses are expanded spatially with a telescope to decrease power/unit area, and are finally sent into a pulse compressor [1].

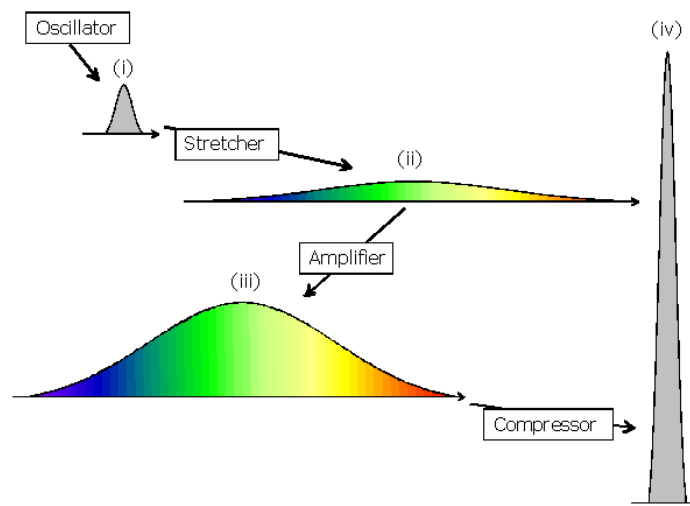


Figure 1.3: Illustration of pulse amplification in a CPA system

Chapter 2

The spatial filter

Standard spatial filters for high power laser systems consist of two lenses, a vacuum chamber and a pinhole. The lenses focus and collimate the beam. The pinhole is placed in the common focus of the lenses to remove the unwanted laser modes. The vacuum chamber is necessary to prevent optical breakdown in air. To be able to understand how a spatial filter works it is important to have some knowledge about how light diffracts, hence a short description of light diffraction under the special conditions of interest will be presented.

Plane waves passing through an aperture will diffract. In the case of laser radiation it is usually the optical components in the beam path that acts as apertures, for instance the active region of amplifying crystals. To the diffraction pattern from plane wave that diffract in an aperture the intensity distribution in the far-field have to be studied. The far-field is where the distance to the source is large enough for the source to be considered to be a single point. A practical way to view the far-field diffraction pattern is to collect the light with a positive lens and to image the pattern in the focal plane.

In some special cases the electric field in the focal plane can be shown to be the Fourier transform of the electric near-field. This is true if the angle of diffraction is small enough and the aperture is small in comparison to the diffraction pattern. This is frequently referred to as the Fraunhofer diffraction condition (The angle of diffraction is small enough if it is possible to neglect the obliquity factor, that takes into account that the light intensity emitted by any "point source" in an aperture is dependent on the angle). We then have

$$E_{far\,field}(k_x, k_y) = \int_{-\infty}^{\infty} \int_{-\infty}^{\infty} E_{near\,field}(x, y) e^{i(k_x x + k_y y)} dx dy.$$

As an example, the Fourier transform of the electric field for a perfect plane

wave travelling through a circular aperture is

$$E(k_\alpha, \alpha) = 2\pi a^2 \frac{J_1(k_\alpha a)}{k_\alpha a}$$

where J_1 is the first order Bessel function of the first kind [2]. The intensity distribution ($I \propto E^2$) is known as the Airy pattern.

The electric field emitted from the aperture can in principle be considered to be built up by several plane waves with slightly different directions, those waves contributing to high spatial frequencies will differ the most in direction.

The size of the far-field diffraction pattern in the focal plane depends, of course, on the lens used. The longer the focal length of the lens the larger the image. The size of a diffraction limited focal spot of a Gaussian beam is

$$\omega_{02} = \frac{\lambda f}{\pi \omega_{01}}$$

where ω_{02} is the beam spot radius in the focal plane, and ω_{01} is the beam spot radius at the focusing lens (from [1]).

2.1 Theoretical analysis of a laser beam propagating through a spatial filter

The light distribution in the focal plane of a focusing lens can be calculated as the Fourier transform of the incoming laser beam, as described above.

The Fourier transform decomposes the laser beam into its spatial frequency components.

Spatial filtering with removal of different frequencies (not only the high ones) can be used for image processing. Filtering of an image can easily be done with a mask matrix, point-wise multiplied with the transform. The structure of the mask determines which frequencies that will be removed. To show how spatial filtering of an image might affect it, an image with a single frequency noise is filtered. The noise introduced here is of one single frequency and can easily be removed. The effect of the filter is clear and practically all the noise is removed, see Figure 2.1¹.

The effect of spatial filtering of different, constructed laser modes (see Figure 2.2), have been simulated. The results are presented in the rest of this section. The high frequencies are removed with a circular aperture in the common focal plane of the lenses, i.e. the intensity matrix for the fast

¹This is a photograph of a piezoelectric controlled mirror mount used in the automatic alignment system discussed later.



Figure 2.1: Original image without noise to the left. Image with introduced high frequency noise ($\lambda_{noise} = 2$ pixels). Spatially filtered image to the right.

Fourier transform (FFT) is set to zero symmetrically around its centre and then inverse transformed. Parameters for the simulations are chosen to mimic the spatial filter studied in this report, i.e. a beam with diameter 8 mm is passed through the spatial filter which uses a $f = 1.5$ m lens to focus the beam. This information is used to get the length scale relation between the near field and its Fourier transform (in the focal plane). A top hat's frequencies are known and described by the Airy pattern. For example, the minima of this pattern can be used to get the length scale of the transformed images used to calculate the pinhole/mask diameter. The modes in figure 2.2 are 80 pixels wide, each pixel represents 0.1 mm. The modes are an almost circular top hat (but with smooth edges instead of sharp) with an intensity value half the value of the hotspots. The types of hotspots in the modes are:

- Mode 1: 0.1 mm and 0.4 mm hotspots
- Mode 2: 1 mm hotspots
- Mode 3: 1.5 mm hotspots

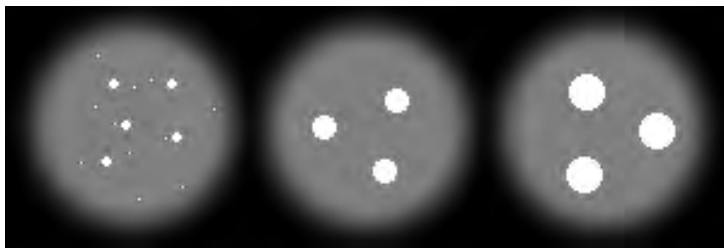


Figure 2.2: From left to right. mode 1, mode 2 and mode 3

The filtered modes can be seen in figure 2.3 to 2.6, corresponding to pinhole diameters of 0.37mm, 0.5mm, 0.6mm and 0.7mm, respectively. The

pinhole with diameter 0.37 mm corresponds to the first minimum in the Airy pattern. The intensity in all the images is completely arbitrary. For the smallest pinholes most of the higher frequencies of the top hat is removed and a Gaussian like profile is achieved. For the larger pinholes some of the frequencies building up the flat "surface" of the top hat are not removed, hence an intensity fluctuation in the beam cross section is introduced, see Figure 2.6 left image. For all pinholes the hotspots are almost completely removed. In the Lund laser system the profile of the near field has a more Gaussian like profile than those modes simulated.

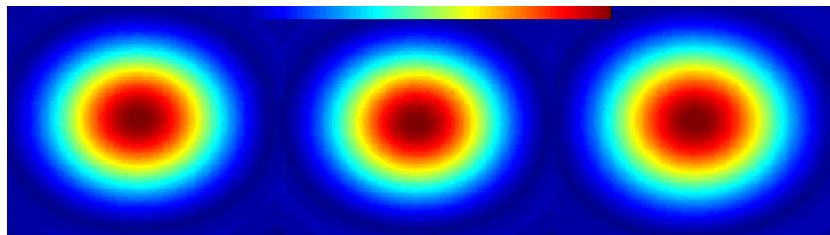


Figure 2.3: Mode 1, 2 and 3 filtered trough a 0.37 mm pinhole

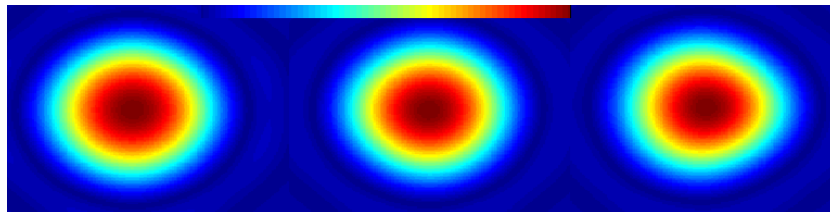


Figure 2.4: Mode 1, 2 and 3 filtered trough a 0.5 mm pinhole

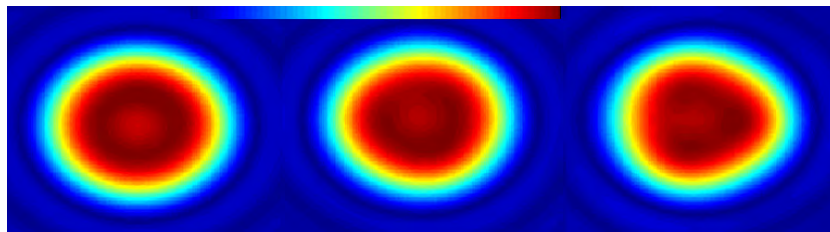


Figure 2.5: Mode 1, 2 and 3 filtered trough a 0.6 mm pinhole

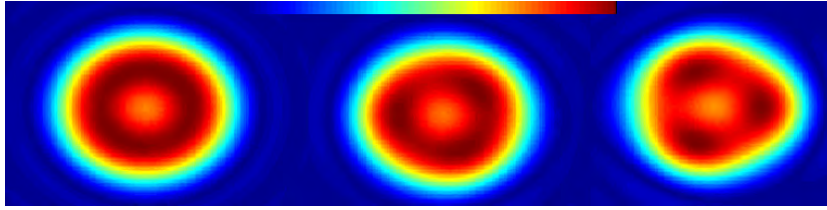


Figure 2.6: Mode 1, 2 and 3 filtered through a 0.7 mm pinhole

Due to energy conservation the total amount of light before and after a lens is unchanged, i.e. the sum of all values in the transform matrix, and the sum of all values in the far-field matrix, should be the same. However, due to edge effects in the FFT the sum of all pixels before and after the transform will differ and this method cannot be used to calculate the intensity loss for different spatial filters. It is the high frequencies induced by the FFT that will have this effect. In the real laser system measurements of the pulse energy before and after the spatial filter showed that 20% of the pulse energy was removed with a 0.6 mm pinhole.

A pinhole of 0.6 mm has previously been used and in this simulations this diameter seems to remove sufficiently high spatial frequencies. In comparison to these simulations, real laser modes (collected from the laser system) filtered through different types of pinholes of diameter 0.6 mm, are presented in Chapter 4.

2.2 Problems with the old spatial filter

The beam direction in the laser system before this project had a certain drift due to temperature variations. This drift causes the focal spot in the spatial filter to move and when the focal spot does not hit the pinhole at its centre less energy will be transmitted through. Higher spatial frequencies will also be transmitted when this is the case. To correct this problem an automatic alignment system has been built. There are also variations in beam direction on a shot-to-shot basis, and some improvements on this issue have also been made. Both these properties will be discussed in more detail in Chapters 3 and 4.

In addition, there has been a small problem with astigmatism in the laser beam, introduced in the first multi-pass amplifier (see Figure 1.2). This results in difficulties in the spatial filtering due to two focal planes separated by a couple of cm in the beam direction so that the pinhole had to be placed somewhere in between (This astigmatism can be seen in figure 2.8 where the

intensity of the beam is collected in the focal plane). Not only the filtering is affected by this problem, in all experiments a small single focal spot is desired. The problem with astigmatism can be almost completely solved if the alignment of each pass through the amplifying crystal in the multi-pass amplifier is perfect. To align the amplifier so that no astigmatism is introduced is concerned with practical problems.

2.3 Problems induced with spatial filtering

Inserting a spatial filter in the beam path will increase the beam quality significantly, especially if there are large intensity variations across the beam, such as hotspots. However inserting transparent material such as lenses will have some small negative affects as well, briefly described in this section.

2.3.1 Dispersion

In all optical materials there is a dependence of the refractive index on the wavelength. This will cause a difference in speed for various wavelength components of the light. This is known as dispersion and is defined as $dn/d\lambda$. For most materials, light with long wavelength travel faster than light with short wavelength, this is called normal dispersion. The dispersion for an optical system is often described in an empirical way, where a power series is used to describe the dispersion dependence of wavelength. The dispersion introduced for a beam passing through the system can be represented as a frequency dependent phase shift δ .

$$\delta(\omega) = \delta_0 + B_1(\omega - \omega_0) + B_2 \frac{(\omega - \omega_0)^2}{2!} + B_3 \frac{(\omega - \omega_0)^3}{3!} + B_4 \frac{(\omega - \omega_0)^4}{4!} + H.O.T.$$

where B_i is called first, second and third order dispersion constant and so on [3].

When the pulses are compressed in a grating compressor (as in this laser system) most of the dispersion induced in the entire system is compensated for. However, since the dispersion introduced has high-order dispersion components and the grating compressor has its own dispersion with high-order dependence it is not possible to compensate completely for the introduced dispersion. The effect of the introduced higher order dispersion is increased pulse length after compression. This is obviously not desirable. Therefore one is trying to keep the amount of material in the beam path as low as possible.

With the spatial filter additional transparent material is inserted in the beam path hence changing the dispersion. The amount of extra glass inserted is due to the two lenses and Brewster windows in the spatial filter. Compared to the total amount of glass in the system (other Brewster windows, lenses, amplifying crystals, etc.) this is quite small. It is hard to predict how this affects the pulse length and the easiest way to find out is to measure the pulse length with and without spatial filter.

Propagation time difference

Two lenses is the easiest setup for a spatial filter. However two positive lenses will cause a small delay in the pulse front compared to the phase front depending on the distance from the optical axis through the lens. The part of the beam at the axis will travel through more glass where the group velocity is less than in air and will therefore be delayed, compared to the parts of the beam travelling through the edges of the lens. This effect (propagation time difference) will cause a temporal stretching of the beam in the focus. For systems with high $f_{\#}$ (focal length/beam diameter) the propagation time difference will be quite small, however not negligible. To calculate the relative delay for the central parts compared to the edges of the beam, for thin lenses, the following formula can be used

$$\Delta t(r) = \frac{-\lambda \frac{dn}{d\lambda}}{2cf_1(n-1)} \left(1 + \frac{f_2}{f_1}\right) r^2$$

where f_1 and f_2 are the focal lengths of the lenses, $dn/d\lambda$ the dispersion of the lens material and r the beam radius (from [4]). Figure 2.7 shows the induced time delay in the present spatial filter. It can be seen that the relative delay (central part of the beam compared to the edges) for this system is only about 1 fs (4 mm radius of the beam before and after the spatial filter). If pulse duration is lowered in the future this time delay might be a problem.

The propagation time difference can be compensated for by inserting negative lenses together with the collimating lenses (same as for achromatic doublets)². This would, however, lead to increased dispersion.

Using mirrors to collimate the beam is an option that does not introduce different delay for different parts of the beam or change dispersion. One of the drawbacks with mirrors is the complexity of the setup. Off-axis parabola mirrors (such mirror has to be used to direct the beam into the spatial filter) are very sensible for misalignments and this give rise to spherical aberration.

²With achromatic doublets the outer parts of the beam is also delayed. This delay compensate for the one induced in the positive lens

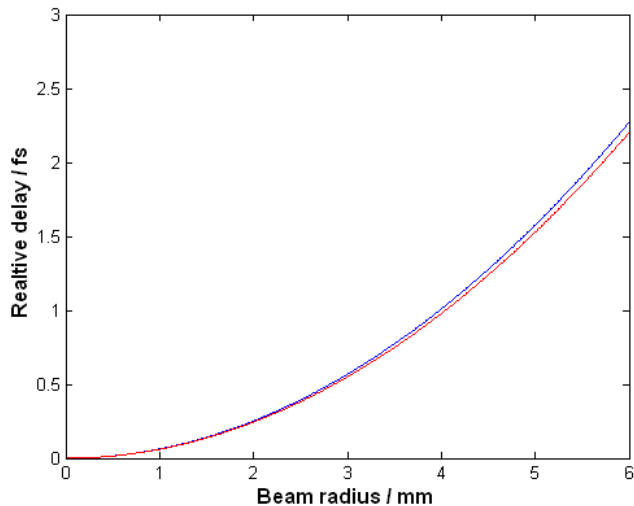


Figure 2.7: Relative delay for central part of the beam for passed trough two lenses made of BK 7 glass (upper curve) and fused silica (lower curve)

2.3.2 Back-scattered light

From all optical components mounted normal to the beam path back reflexes are created. This might cause problems if the reflected beam is amplified on its way backwards and a risk of damaging optical components is introduced. The lenses in the system used today are there for anti-reflection coated and slightly tilted to minimize this problem.

2.4 Pinhole

In the pinhole the high spatial frequencies of the laser beam are removed. The conventional design of a pinhole is a metal plate with a circular hole. At the edge of the hole where the unwanted light is absorbed, plasma can be generated. The plasma will ablate material and eventually the size of the pinhole will increase, affecting its functionality. These types of pinholes only have a limited lifetime depending on pulse energy and the amount of filtering.

There are also other problems with beam quality associated with the formation of plasma, this is described in the Section 2.4.2.

Pinholes made of other materials than metal might be possible to use. Trials with such a pinhole have been made and reported in [5]. It was decided

to test similar pinholes (conical pinholes of glass) in this project to prevent formation of plasma. Hence in the next section formation of plasma threshold values for dielectrics are discussed.

2.4.1 Formation of plasma

With conventional pinholes in high power laser system, plasma will be generated at the absorbing surface and a small amount of material will be ablated at each pulse. However, as mentioned above, it might be possible to create pinholes made of dielectric material with high plasma threshold that will prevent plasma formation. Threshold values for dielectrics are therefore discussed in this section.

For dielectric material, at the threshold of plasma formation, avalanche ionization is the dominating absorption mechanism ($\lambda = 800$ nm, $\tau = 260$ ps and pulse energy = 500 mJ). For dielectric material in the avalanche ionization regime the threshold (F_{th} , energy/unit area) for plasma formation is proportional to the square root of the pulse duration ($F_{th} \propto \sqrt{\tau}$) for pulse length of 10 ps up to nanoseconds [6] [7]. This proportionality can theoretically be explained by considering the thermal damage dependency on the thermal diffusion length [6]. In the avalanche ionization model the plasma threshold is determined by the electric field in the material. The mean collision time of the electrons is short in comparison with the laser frequency and hence the drift velocity of the electrons, and their energy, can be considered constant during one period of the laser. The threshold will thus be the same as for a static electric field (for pulses shorter than 10 ps there is no heat transfer into the crystal lattice and the threshold dependence of pulse duration will change from the root dependence of pulse width).

The plasma threshold for a surface is always considerably less than for the bulk material and therefore it is at the surface the breakdown will occur. Measurements on plasma threshold values for different dielectrics have been performed by several groups. In reference [6] measurements on fused silica glass (SiO_2) have been performed with pulsewidths from femtoseconds up to nanoseconds. For pulses of 260 ps (as in our system) F_{th} is estimated to 25 J/cm² at normal incidence (wavelength 800 nm). In reference [5] the threshold for NG-4 glass (absorbing ND filter) is measured to 80 J/cm² for 4.5 – 5 ns pulses for normal incidence. The corresponding value for 260 ps would be 20 J/cm² if $F_{th} \propto \sqrt{\tau}$ is considered. This is similar to the value presented in [6]. Thresholds for grazing incidence has also been measured, for 2 degrees a threshold of 3000 J/cm² and for 9 degrees a threshold of 500 J/cm² are presented in reference [5]. The corresponding values for 260 ps pulses are 700 J/cm² and 120 J/cm² respectively. These values are measured for

P-polarization (worst considerable), see Figure 2.12. Reference [8] suggest a higher *intensity* threshold for glass than for fused silica, 2.8×10^{13} W/cm² compared to 1×10^{13} W/cm², for a 120 fs (FWHM) pulse.

Research has been done also on deterioration of optical material in sub threshold laser fields. If a large enough number of pulses hit the material it may cause damage even for fields far below the threshold, as low as $0.6F_{th}$ is suggested by reference [9]. However reference [6] suggests same thresholds for multiple pulses and single pulses. In our spatial filter a very large number of pulses will hit the pinhole with just below plasma threshold so if there is such a mechanism in process this will be a problem. How big the problem is and if the damage is larger than that caused by the few pulses that will miss the pinhole, has to be tested on the real system. Even if tested it will probably not be possible to determine which process actually caused the damage.

If the glass surface is contaminated its plasma threshold is dramatically lowered. Reference [10] presents decreased values for glass contaminated with steel. This might be an issue if dirt on the absorbing surfaces in the pinholes is present.

The dominating mechanism of absorption for formation of plasma in stainless steel is multiphoton absorption ($\lambda = 800$ nm, $\tau = 260$ ps and pulse energy = 500 mJ). Plasma threshold for stainless steel is significantly lower than for dielectric material. Reference [11] suggest $F_{th} = 0.16$ J/cm² for 150 fs and wavelength of 775 nm and reference [5] suggests lower thresholds in the nanosecond region.

2.4.2 Plasma closure

When plasma is generated on the edges of the pinhole it will expand into the hole affecting the pulses. If the electron density is high enough it will cause plasma closure. Plasma closure is the term used when only a fraction of the beam is transmitted through the pinhole. The speed of expansion is dependent on electron temperature and the material that forms the plasma. The speed of plasma (v_p) expansion is proportional to

$$v_p \propto \sqrt{ZT_e/M}$$

where Z is the charge state, T_e the electron temperature and M the atomic mass [12]. Materials with high atomic mass can be used as pinhole material to decrease the speed of the plasma. The term ZT_e can be decreased if lenses with longer focal length is used or if the incident light is hitting a surface at grazing incidence, resulting in less absorption per unit area. Closure time

for a pinhole of the same diameter as used in this system has been measured to about 2 ns, according to reference [13]. Reference [14] has measured plasma closure velocity to 2 to 5×10^7 cm/s in the same conditions. In these two cases long (ns) pulses were used. For long pulses the plasma created is further heated by the later part of the pulse. This will cause a higher electron temperature for both these measurement, probably significantly higher than those plasma temperatures considered in this system.

It is the electron density that affects the beam causing a phase shift. The phase shift (δ) dependence on electron density is:

$$\delta = \frac{\pi}{\lambda} \int_0^L n/n_c dz$$

where n/n_c is the ratio of electron density and critical density (where the plasma frequency equals the laser frequency) [13]. The critical density is given by:

$$\omega_p^2 = n_c e^2 / \varepsilon_0 m$$

where ω_p is the frequency, m is the electron mass and ε_0 is the electric susceptibility (from [15]). For $\lambda = 800$ nm, $n_c = 1.7 \times 10^{21}$ /cm³. The phase shift created may cause spatial intensity fluctuations in the near field, higher spatial frequencies, and this is exactly what the pinhole is meant to remove. The functionality of the spatial filter is apparently reduced when phase shift occurs in the pinhole. Plasma closure is mainly a problem for longer pulses. The stretched pulses in this laser system, when passed through the spatial filter, are only 260 ps long.

2.4.3 Geometrical designs and material of the pinhole

It might be possible to design a pinhole that could withstand higher laser intensities without plasma formation and therefore would not have to be exchanged as frequently as conventional pinholes. To design such a pinhole the geometrical shape and the material selected is crucial.

The typical fluence in the focal plane in this system at the edges of a 0.6 mm pinhole is presented in figure 2.8. These values are estimated to be valid when the pulse energy passed through the spatial filter is 500 mJ. To estimate these values the focal plane in the spatial filter has been imaged on a CCD camera. Because of the shot-to-shot variation, of the focal spot, the pinhole will never be perfectly aligned and practically all pulses will slightly miss the centre of the pinhole. Hence the maximal value for each pixel on the CCD for several (6) collected pulses are recorded. Linear response for the CCD camera is assumed when the pixel values are transferred to energy density.

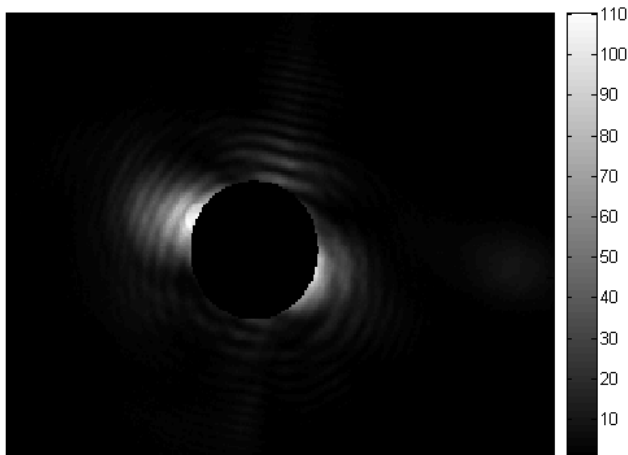


Figure 2.8: Fluence (for pulse energy of 500 mJ) in J/cm^2 at the edges of a 0.6 mm pinhole.

Conical pinhole

To decrease plasma formation it is possible to change the geometrical properties of the pinhole. In a conical pinhole (schematic pinhole in figure 2.9) the light hit the surface at a small grazing angle. This leads to higher reflectivity and the surface would be subjected to less radiation per unit area, compared to a surface normal to the beam, see Figure 2.12. Threshold values for grazing incidence light has been measured by [5] and discussed in this report in Section 2.4.1. Absorption is also dependent on the surface material and its smoothness. For a conical pinhole to have the same filtering effect to the beam as a conventional, no reflected or refracted light is to be collected by the lens after the pinhole. The angle α is therefore restricted to:

$$\alpha_{min} = d/2f$$

where d is the beam diameter on the lens and f the focal length. Externally reflected light is phase-shifted 180 degrees and this might cause an intensity modulation in the near field just as in the case of plasma closure.

To decrease the fluence, light should not be reflected more than once inside the pinhole. If it would be, it would add up to the intensity close to the exit hole (at the edge of S_1 and S_2). This leads to the restriction

$$L < \frac{d_{in} + d_{out}}{d_{in} - d_{out}}$$

where d_{out} and d_{in} is the exit and entrance diameter of the pinhole.

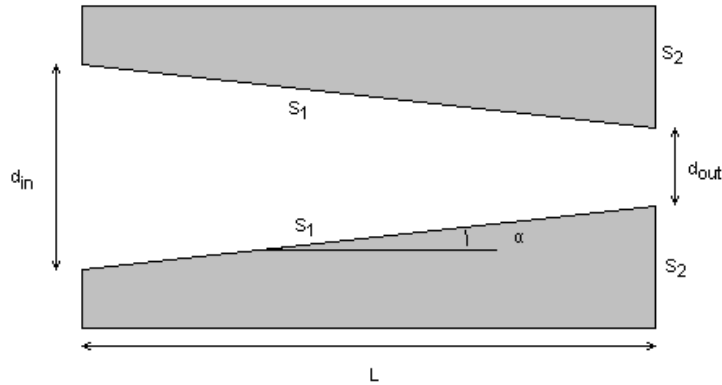


Figure 2.9: Conical pinhole

With intensities as high as in the Lund terawatt laser system with a focusing lens of 1.5 m and pinhole of 0.6 mm it is not possible to prevent plasma formation in a stainless steel pinhole. This is due to the restriction $\alpha > \alpha_{min}$ and limits in surface smoothness. For a conical pinhole in stainless steel it is possible to decrease the plasma temperature and the problems concerned with this, plasma closure. However, for a conical pinhole there is less material at the exit that can be ablated before the pinhole has to be refitted compared with a conventional pinhole. Hence for laser systems like the present one there would be no benefits with a conical pinhole made of metal.

If the pinhole is made of a dielectric material with high damage threshold it is possible to decrease fluence below plasma threshold (F_{th}). Glass, for instance, can be fabricated with a very smooth surface in combination with a small angle α and absorption can thus be greatly reduced. Heating and stretching of a glass tube to the dimension desired is the most promising method to fabricate such pinholes. To polish a glass surface to the same smoothness obtained with stretching is very difficult. The reflectivity dependence on incident angle for S- and P-polarization in glass can be seen in figure 2.12. Light refracted into the glass will exit the pinhole at surface S_2 at normal incidence and it will also interfere with reflected light at the same surface. This means that this surface is the most exposed and will be the first place where plasma is generated. If the values of F_{th} in section 2.4.1 are valid (around 20 J/cm^2) the fluence at surface S_1 will be well below F_{th} when the angle α is reasonable small in the pinhole. A slope of 1/10 is enough to guarantee this (fluence at normal incidence is about 110 J/cm^2 , from figure

2.8). At the surface S_2 the fluence will be above F_{th} for $\alpha >$ about 1 degrees (90% reflectivity according to figure 2.12)

A solution to this problem is to create a pinhole with $\alpha > \alpha_{min}$ and symmetry around the focal spot. Exact symmetry is not required but a slope with small enough angle to decrease the fluence to below damage threshold is needed. See figure 2.10. However such a pinhole would be much harder to fabricate than just a simple cone. It is almost impossible to stretch a glass tube to form a sharp waist in the middle (sharp waist required to minimize collected reflected light). A more promising method is to polish the surface at the exit hole to the desired slope. The fluence on surface S_3 will be reduced below F_{th} if angle β is small enough and good enough smoothness is obtained on surface S_3 .

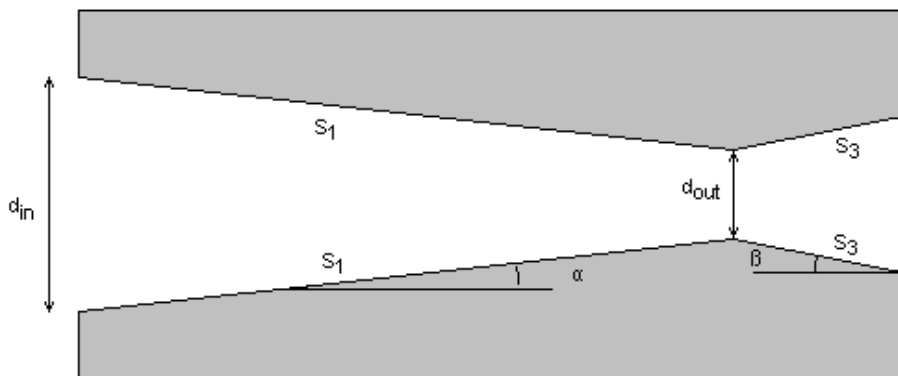


Figure 2.10: Schematic picture of conical pinhole

There is unfortunately also a disadvantage with conical pinholes, the alignment is crucial for it to work properly. This is not only to prevent plasma formation. Especially for pinholes with a small angle α it is important that the pinhole is aligned almost exactly along the beam so that no reflected light is collected by the lens after the pinhole. This is a drawback with this type of pinhole and no really good method for aligning it has been developed. However to make the alignment easier the conical pinhole is mounted on a Gimbal mirror mount in combination with a simple cylindrical device, see figure 2.11. The exit tip of the pinhole is placed in the middle of the tilting surface of the mirror mount. A Gimbal mirror mount tilts the mirror surface around its centre without changing its coordinates in space. This property makes the pinhole tilt around its exit hole without changing its position.



Figure 2.11: Conical glass (Borosilicate) pinhole. And holder for the pinhole to the right.

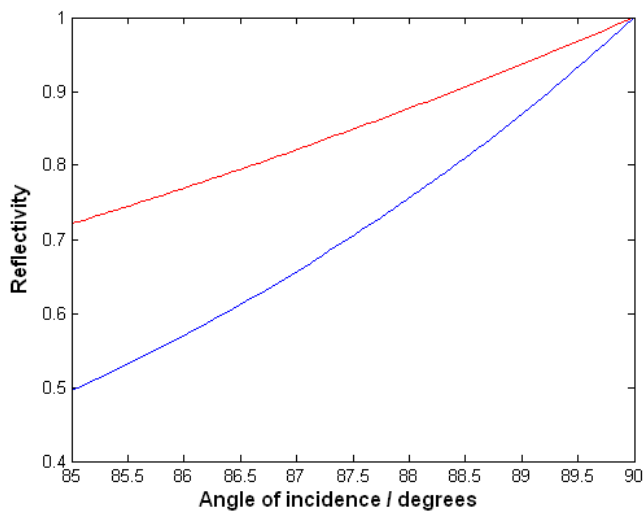


Figure 2.12: Reflectivity for polarized light glass (borosilicate, $\lambda = 800$ nm). Upper curve, S-polarization. Lower curve P-polarization.

2.5 Vacuum chamber

The vacuum chamber used in the old spatial filter consists of a stainless steel tube fitted with fused silica windows (at Brewster angle) at its end spots and a larger chamber in the middle where the pinhole is fitted. There has been no modification made on this part. An advantage with the collimating lens before the vacuum chamber is the simplicity of the setup. The possibility to sample the beam for the detection system which is connected to the control system after the focusing lens, is another advantage (However for now this is not done). The disadvantages with this setup are that extra material are inserted into the beam path which contributes to dispersion (see Section 2.3.1). Variations in atmospheric pressure will influence the refraction angle through the air-glass-vacuum interface and this will cause the focal spot to move slightly when the surrounding pressure is changing. This variation can be calculated with Snell's refraction law. The refractive index in air dependence of pressure is linear for the pressures considered. At normal atmospheric pressure the refractive index of air is 1.00029, i.e.

$$n_{air} = 1 + \frac{0.00029}{101300}p$$

where p is the pressure in Pascal. The deflection of the focal spot due to varying air pressure is presented in figure 2.13. Here it can be seen that the variation can be as large as 20 μm in the focal plane. However, this is no problem of greater concern as long as the length of the vacuum tube is not increased. Deviations larger than 10 μm will be rare and such small variations will not affect the functionality of the spatial filter.

An alternative setup, to the vacuum chamber confined by two Brewster windows, would be to attach the lenses directly to the vacuum chamber. However, for this system little is gained with this modification.

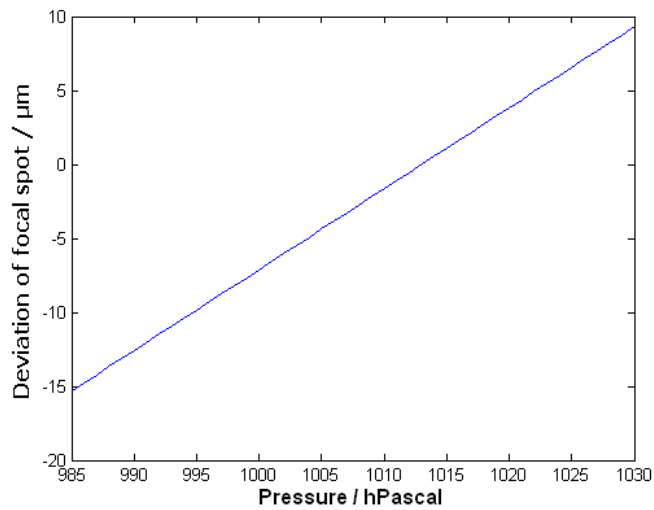


Figure 2.13: Deflection of the focal spot in the pinhole as a function of atmospheric pressure

Chapter 3

Automatic alignment

In order for the spatial filtering to work properly it is important that the focal spot is located at the centre of the pinhole and does not change its position with time. A drift of the beam direction caused, prior to this project, the focal spot in the pinhole to move. This drift is now compensated for via an automatic alignment system that controls the tilt of a mirror (mirror M_1 in figure 1.2). The sensor that gives the error signal is mounted in an equivalent focal plane as the pinhole (CCD detector in figure 1.2). The direction stability in time is important for several reasons, not only for spatial filtering. But also the direction through other optical components such as amplifying crystals. The mirror M_1 controls the direction into the multi-pass amplifier (see Figure 1.2). The spatial filter and the automatic alignment system associated with it are both placed on the second optical table (in figure 1.1) and fixes the beam direction relative to this table. Parts of this second table is presented in the schematic view in figure 1.2.

Turbulence in the air causes a variation of the beam direction on a shot-to-shot basis. This effect does not only affect spatial filtering but also the centre calculation of the focal spot.

For the control system a standard PC with LabView installed is used for all data processing and communication with the camera and the digital to analog (D/A) converter. An high voltage amplifier (-30 to 150 V) is used to amplify the signal from the D/A converter. The mirror controlled (M_1 in figure 1.2) is mounted on a piezoelectric controlled mirror mount (photographs of this mount can be seen in figure 3.6 and 2.1). The control signal (the amplified signal from the D/A converter) is directly applied to the two piezoelectric crystals. The control signal is calculated in the computer after image processing of the image received from the camera.

In this section the automatic alignment system used is described.

3.1 Beam drift

During operation of the laser the beam changes direction. The changes are slow (compared to the laser repetition frequency) and are easily compensated for by the alignment system. The changes can be explained by temperature variations, mainly from; ventilation system, absorption of laser light, heating from electrical power consumption and personnel. All these affect the entire optical table as well as components in the beam path. A measured beam drift (of the focal spot in the spatial filter) during the first 5 hours of operation of the laser can be seen in figure 3.1. This drift is very similar from day to day. Most of the drift is introduced early in the system, before the first "butterfly" multi-pass amplifier. The drift on the controlled mirror is almost only variations in direction and not in position of the beam, hence it is possible to use it to align the multi-pass amplifier as well as the spatial filter.

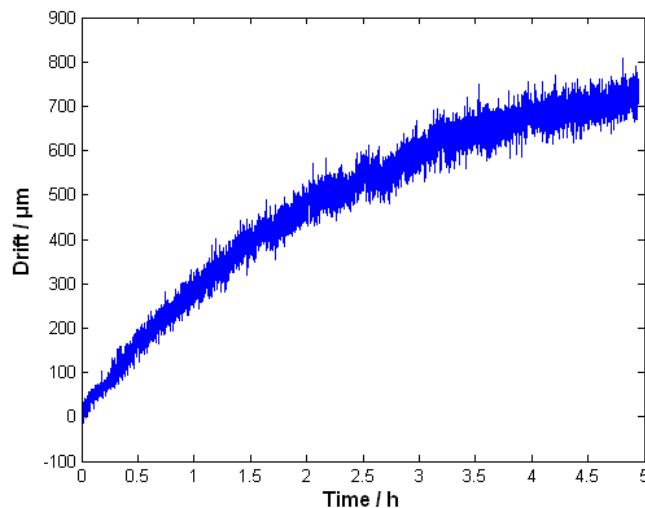


Figure 3.1: Drift of the laser beam direction during first 5h after start-up.

3.1.1 Shot to shot variations in the beam

Movement of air in the beam path is causing a fast but small variation in the beam direction. This variation is almost random from shot to shot and therefore it cannot be compensated for in the control system. See Figure 3.2 where the focal spot position in one direction is measured. The behaviour for the shot-to-shot variation in both the x- and the y- direction is similar.

Minor improvement is however achieved with the control system running. The problem tends to increase when the laser system has been in operation for several hours. As the laser normally operates for several hours this is a problem. The reason is probably a result of higher air temperature in the beam path and variations in the air conditioning system during the day. Ventilation is increased as the room temperature is rising due to heat emitted by the laser system.

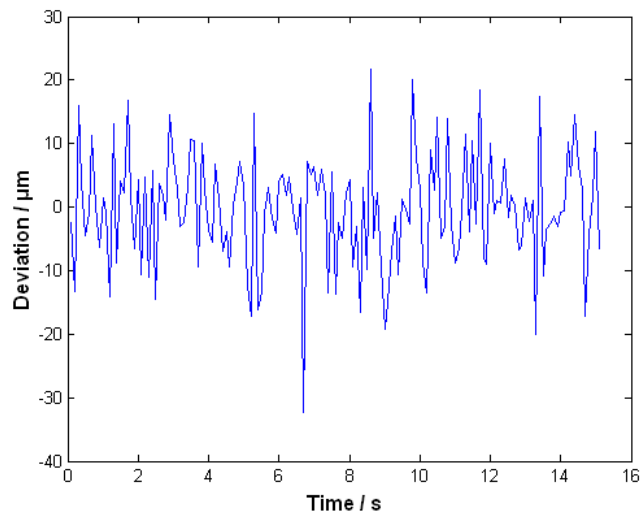


Figure 3.2: Focal spot position in the x-direction during 15 s.

The variation in beam direction directly causes a variation of the focal spot in the pinhole creating problems with spatial filtering. Full-width-at-half-maximum (FWHM) of the focal spot is about $300 \mu\text{m}$, the pinhole is $600 \mu\text{m}$ and the variation from shot to shot is of the order of $20 \mu\text{m}$. See Figure 3.3.

Measurements have been made to determine where the variations originate and it is shown that the problem occurs after the first (regenerative) amplifier. In this amplifier a laser cavity is used and only specific laser modes are amplified. The amplification is of the order of 10^6 . Due to this the beam exiting this amplifier is very stable and no shot-to-shot variation in direction is present.

There is an easy solution for the shot-to-shot variation problem; confine the beam path. For example screens and tubes can be used. Some confinements have previously been done to the system, almost the entire system, from the first amplifier (regen) to the spatial filter is enclosed in a single

box, see Figure 3.4. This box is reducing air movement very efficiently. See Figure 3.3 for variation in focal spot position in the spatial filter without the box. To divide the box in smaller sections and to let the beam travel through pipes where it is possible would decrease the variations significantly. Trials with screens and pipes have been done and the results are clearly shown in figure 3.3. Here approximately 2.5 m of the beam path previously in free air was enclosed in tubes. The two logs, with and without tubes, were collected only minutes apart and for such short time intervals the behaviour of the laser is in practically unchanged.

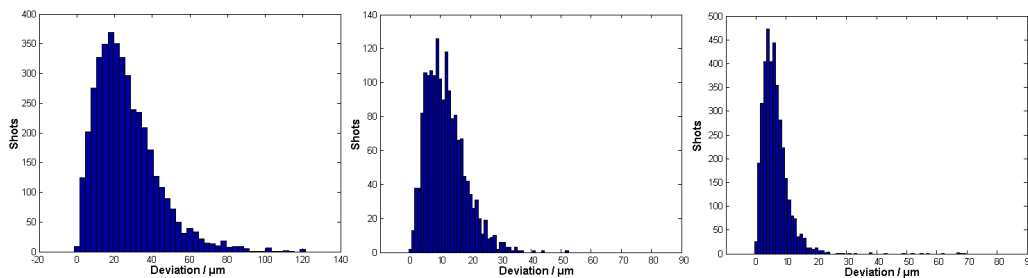


Figure 3.3: From left. Histogram over total error when the protecting box is removed. Middle. Histogram over total error with beam passing through open air. And to the right when approximately 2.5 m of tubes are used to confine the beam path.

3.2 Choice of fixed points in the laser system

In this project it has been decided that only the focal spot at one place in the beam path should be fixed via the control system. This fixed point is the focus in the spatial filter, which is enough to guarantee the functionality of the filter. However the beam position may vary and still hit the same focus, i.e. have the same direction. Not only the direction through the first multi-pass amplifier on optical table 2 (Figure 1.2) but also the position of the beam is important for the amplification. Today the alignment of the beam position into and out from this amplifier is done manually via two apertures (A_1 and A_2 in figure 1.2), one just before and one after the amplifier. If they are hit correctly the beam position through the amplifier will be correct.

The choice of which mirror to control has been a compromise regarding the spatial filter alignment and has partly a historical reason. This mirror (M_1) has previously been used for the daily manual alignment due to drift.



Figure 3.4: Photograph of the box covering parts of the laser system.

The reason the compromise has been made is that it is desirable to use the alignment system not only for the spatial filtering but also for the alignment through the first amplifier, which in the past has proven to work well. The mirror controlled is the one just before entering the amplifier. As mentioned earlier in section 3.1 this is possible because the drift is induced close to, or after, this mirror and hence the position of the beam is almost unchanged. This is considered the most efficient way to use the equipment.

3.3 The detection system

For the automatic alignment system to work some sort of error signal has to be obtained when the alignment of the spatial filter is incorrect. To be able to do this some kind of detection system is needed.

When deciding which detection system to use several desired criteria were considered.

- A precise and robust detection of the focal spot position was required. For example dust on a mirror affecting the intensity distribution on the detection system should not affect the measured position of the focal spot.
- Detect short pulses of infrared.

- A reasonable spatial resolution was desired to get some more information about the beam properties than its direction, for example; possible astigmatism or the amount of higher spatial frequencies.
- Triggering to detect a single shot. If a pulse has not been detected each time the detection device sends unnecessary data processing would have to be performed. And the speed of the alignment systems would be decreased.
- Easy to connect and use the information sent from the device.
- Low total cost.

All these criteria have led to the decision that a CCD camera is the best choice. CCD cameras with the computer interfaces firewire and USB are at a reasonably low price and no specialized control hardware is needed for the computer connection. The choice between USB and firewire fell on firewire because this interface follows a standard digital camera specification, this is not the case for USB where each manufacturer uses its own specifications. With firewire cameras the same software driver can be used for all cameras.

The final choice of camera fell on a CCD-camera with a 1/3" chip with a resolution of 640×480 pixels. The size of each pixel is roughly $10 \times 10 \mu\text{m}$ and with this chip it is possible to determine the focal points position with an accuracy in the order of a few μm . This is enough precision for the spatial filtering. The CCD's sensitivity for infrared light is not an issue, as long as the CCD chip is not coated with an IR absorbing filter, because of the high laser intensities available in the laser system.

To monitor the beam the simplest and most exact way is to focus the beam directly on the CCD chip. One might expect problems with interference between the different layers in the CCD but due to the large bandwidth of the laser pulse this problem is eliminated. An example of how the beam appears on the camera can be seen in figure 3.5. Here diffraction patterns from dirt on filters and on the CCD chip can clearly be seen.

3.3.1 Detection of the beam

To detect the beam different methods have been considered:

- Inserting a glass plate placed after the focusing lens L_1 at almost Brewster angle
 - using the leakage from a mirror placed after the focusing lens L_1
-

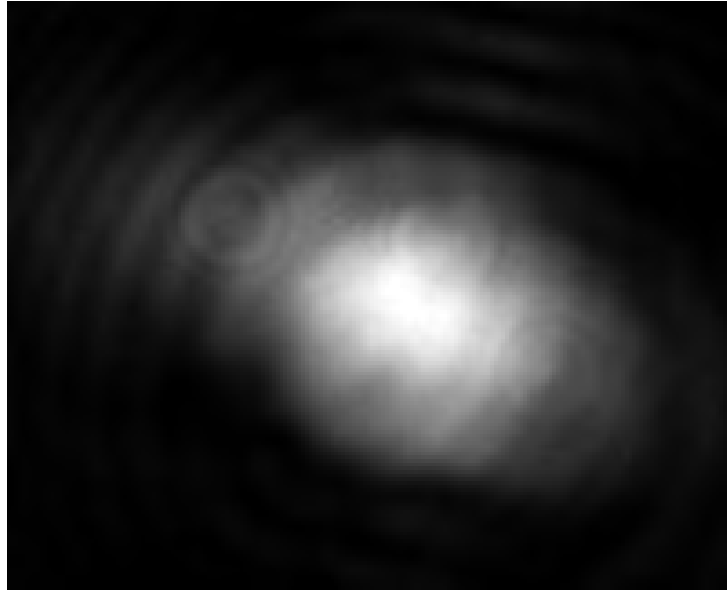


Figure 3.5: Sampled pulse

- using the leakage from mirror M_2 , before the spatial filter, in combination with a separate focusing lens L_3 .

The first two cases have an advantage that the camera will image exactly the same focus as the pinhole is seeing. The first case where a glass plate is placed in almost Brewster angle just after the spatial filter focusing lens, before the vacuum chamber has been tried in practice. Problems with stability were observed. Hence this setup is not used today. A second disadvantage with a glass plate sampling the beam is the extra material inserted in the beam path affecting the dispersion.

>From a dielectric interference mirror there is always a small leakage, this leakage can be collected and used for the detection system. If a mirror is placed after the lens L_1 , the leakage can be collected directly on the detector. An alternative setup is to use the leakage from the mirror M_2 , just before the spatial filter lens L_1 , and place a second lens L_3 with the same focal length as L_1 after the leaking mirror to produce a focal plane on the CCD. An advantage with these two arrangements is that no extra material is inserted in the beam path. If the reflecting coating is burned on a mirror it will transmit all light in this region, which might cause a problem with too high intensities for the camera. However a CCD chip is not very vulnerable for high intensities and this should not be a problem. In the second case a separate lens is used to focus the beam onto the camera and it is important

that the alignment of this lens is correct so that the focal spots of the two lenses do not move relative to each other if the position of the beam changes.

In all these cases it is desirable to place the camera physically as close to the pinhole as possible. This is because movements in the optical table should not affect the measured focal spot coordinates ¹. The alignment system controls the beam according to the movement of the focal spot on the CCD and if this focal spot and the one in the pinhole could move relative to each other the alignment would fail. It has therefore been decided to use the second alternative, where the leakage of a mirror and two lenses are used (just as in the schematic picture in figure 1.2).

3.4 The control system

To control the tilt of mirror M_1 piezoelectric crystals are used. The voltage applied to the crystals is calculated in a computer, which receives an error signal from the detection device. The calculated control signal is converted to an analogue signal in the D/A converter and amplified in an external amplifier.

How the control signal is calculated and used is described in this section.

3.4.1 Piezoelectric crystals

The structure in piezoelectric crystals is such that an applied voltage will change its length. The typical change in length for a piezoelectric crystal is 2/1000 of its length. The crystals have an almost linear reaction to an applied voltage. There exists also hysteresis and creeping in time of the crystals. Because of the high repetition rate of the laser (10 Hz). Creeping is a slow process and will be compensated for in the control system. The only negative effect the hysteresis has on the function in this case is a small decrease in operating length of the piezoelectric crystals.

To control the mirror two piezoelectric stacks are mounted in a specially designed mount, see Figure 3.6. The length of the piezoelectric stacks is 9 mm and the stroke length is 15 μm [16]. Mounted 25 mm from the tilting point of the mount this gives a maximum angular change of $\frac{2 \times 15 \times 10^{-6}}{25 \times 10^{-3}} \approx 1.2 \text{ mrad}$ which in the focal plane is $1.5 \times 0.0012 \approx 1.8 \text{ mm}$. This is enough to compensate for the daily drift. (However the piezoelectric stacks do not perform this well in practice about 1 mm in the focal plane). The choice of piezoelectric stack length is made considering that the shorter the stacks are the better precision of the beam direction. If the control system by some

¹During the day the optical table twists and bends. If the detection device and the pinhole are placed close to each other the influence of these effects are minimized.

reason fails to work it will not be able for the beam to move outside the active region of the amplifying crystal (in this case the beam will still appear on the camera) and the error will be much easier to find and correct. A disadvantage is that manual adjustments may have to be performed more frequently.

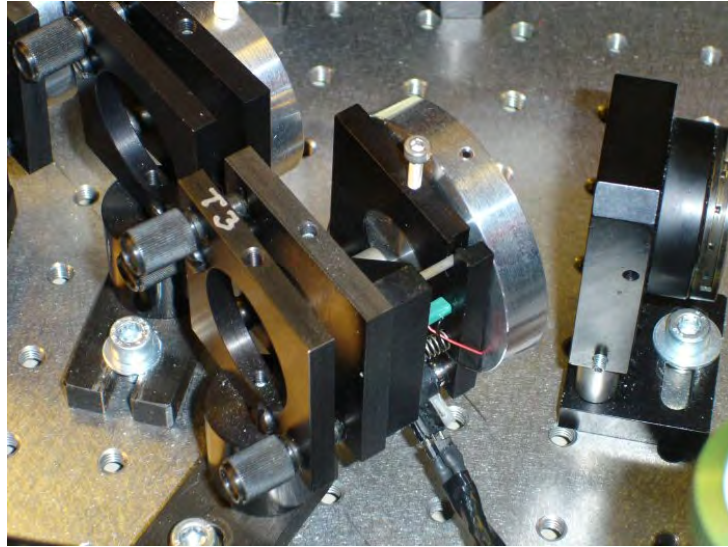


Figure 3.6: Photograph of the specially designed piezo-driven mount between a standard mirror mount and the mirror.

3.4.2 Data processing

As mentioned above, LabView is in this project used to receive, process and send data. A great deal of effort has been made to create a simple and understandable program (Beam Control), which without too much effort can be developed or modified later on. User friendliness and the choice of functions in the program have of course also been main issues. A screen dump of the main window of the Beam Control program can be seen in figure 3.7. Functions implemented in the program are:

- Ability to manually/automatically control the control signal (used to control mirror M_1)
- Ability to send a TTL-signal used to physically block the beam if a control signal is saturated

- Create a log of the beam properties during the day, absolute time, deviations of the beam, control signals, mean and maximal pixel value
- Load and plot the saved logs
- Save snapshots of the beam with 10-bit resolution
- Real-time statistics presented in graphs.

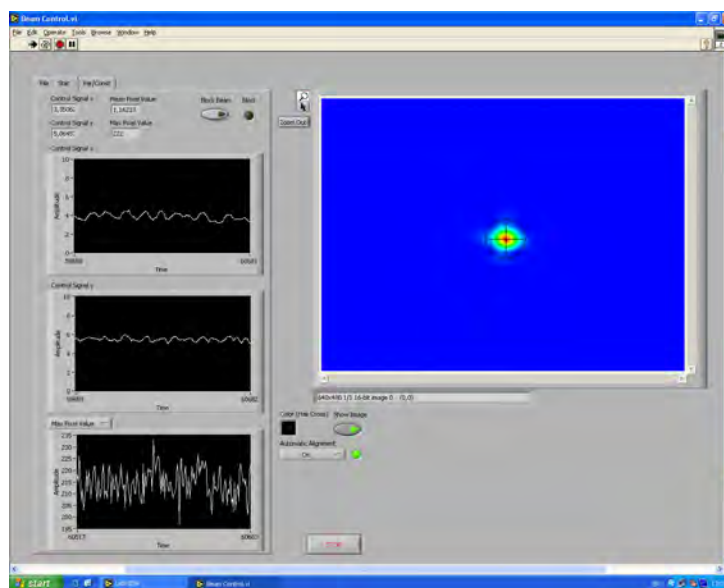


Figure 3.7: Screen dump of the Beam Control program.

Calculation of the focal position

The focal spot on the CCD is roughly $300 \mu\text{m}$ (FWHM), which corresponds to about 30 pixels. Several methods for calculating the centre have been tested; different kinds of function fitting, different threshold levels, different number of thresholds and variations of these techniques. There are obvious problems when trying to fit a function to the beam profile in figure 3.5. Due to diffraction of the beam due to dirt on filters etc, the intensity distribution is often a complicated function and it is hard to fit for instance a Gaussian function to it. In addition, a function fit is a rather time consuming process in the computer and not significantly better than threshold calculations. Therefore this type of focal point determination was abandoned quite early.

Today the mean value of three threshold levels (at 1/6, 1/3 and 1/2 of the maximum pixel value) is performed to calculate the centre. No significant difference can be seen when larger number of threshold levels are used. If a too high threshold value is chosen, diffraction pattern from dust on the filters might affect the centre calculation. To suppress this effect quite low threshold values (a larger area is obtained to calculate the centre of) is taken where small fluctuations from diffracted light have a small impact on the centre calculation. This is why the values mentioned above are used. If the multi-pass amplifier is correctly aligned the phase of the spatial frequencies in the near field is uniformly distributed and hence the focal spot is cylindrically symmetric (perhaps with a slightly oval shape, originating from astigmatism). This is important when low threshold values are used to calculate the centre.

Calculation of the control signal

To calculate the control signal a recursive algorithm is used. The control signal calculated is the previous cycle added with a constant multiplied by the error. In principle the signal is calculated with the formula:

$$S_n = C \cdot \text{error} + S_{n-1}$$

where S_n is the calculated control signal and S_{n-1} is the control signal for the previous cycle. This is a purely proportional and integrating control system and this choice is made in consideration of the linear properties of the piezoelectric crystals used. To suppress the effect of single shots with large error in the control system a median value of the errors of the last three shots is taken. If the median over the last tree measurements is taken the speed of the control system is almost not affected at all.

To determine which proportionality constant C to use, and how many pulses to take the median value of, a trial-and-error method has been used. The parameters have been changed and the ability to adjust the mirror according to the variations present in the system has been studied. This study builds on analysing histograms over the error received for different parameters. The results are discussed in Chapter 4.

Chapter 4

Results and discussion

4.1 The spatial filter

Today the original setup of the spatial filter is being used, where only the part of the beam that will be further amplified is passed through the filter. This means that only about 25% of the energy is transmitted. Changes that have been made on the original spatial filter are modifications of the pinhole. It has been decided to maintain the present setup until the functionality of the new pinholes has been further tested. The latest design of a conical pinhole made of transparent glass is now being tested to evaluate the functionality and the damage caused by the laser in long-term use.

It has been shown that for a conical pinhole with a flat exit surface, (S_2 in figure 2.9) this surface is most vulnerable. It is almost impossible to prevent plasma formation when pulses with energy of 500 mJ are filtered ($d_{out} = 0.6$ mm). With the present setup, with reduced energy (about 125 mJ/pulse), there seems to be no problems with laser induced damage on this surface. Those tests performed on this type of pinhole suffer from the problem to keep the focal point in the centre of the pinhole during the entire test. Most of the damage on the pinholes during the tests occurred when a pulse misses the pinhole.

Different pinholes have been tried in practice. Pinholes with flat exit surface experience the problem mentioned above but is easy to fabricate. Trials have also been made to manufacture pinholes with a waist in the focus but there are some problems both in fabrication and functionality. With the same fabrication methods as for the conical pinhole, i.e. stretched glass tube, it is hard to create a pinhole with a short waist and sufficiently small grazing angle. There are fundamental problems associated with the waist in the middle, light that is reflected close to or at the waist will be collected by

the collimating lens at the end of the spatial filter.

Trials with conical pinholes for spatial filtering have been made to compare the filtering effect with conventional pinholes. All pinholes used in these trials had a diameter of 0.6 mm. Three different pinholes were used; conventional stainless steel, glass with $\alpha > \alpha_{min}$ and $\alpha < \alpha_{min}$. Two different modes have been filtered, one with a thin metal fibre introduced just before the spatial filter and the other without any disturbances. The unfiltered mode can be seen in figure 4.1 together with an image of the metal fibre. (The fibre is here placed close to the beam profiler.) The filtered images are presented in the following figures; 4.2 4.3, 4.4. The tests performed on pinhole with $\alpha < \alpha_{min}$ (see Figure 4.4) show problems with the mode such as intensity modulations in the left figure (very small variation). The mode filtered in this case is very divergent (compared to modes filtered during operation of the system), hence a large fraction of the light will hit and be reflected on surface S_1 (with $\alpha < \alpha_{min}$) and collected by the collimating lens. The intensity fluctuations seen in figure 4.4 are quite small. The size of the problem of collection of externally reflected light when modes with lower divergence (smaller hotspots) are filtered has not been measured. According to these measurements the problem seems to be very limited, if it at all exists. Perhaps small intensity variation can be seen in the left figure 4.2 as well. These would originate from a slight misalignment of the pinhole. The phase shifted light might perhaps have other negative effects as well for some applications of the laser.

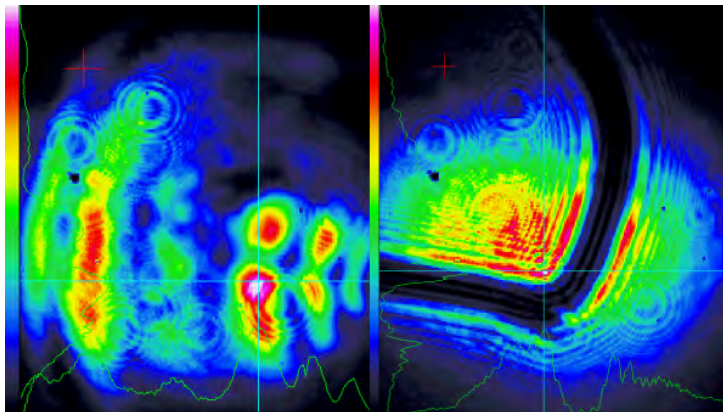


Figure 4.1: To the left, the unfiltered mode with a metal fibre introduced in the beam path before the spatial filter. To the right, image of the metal fibre used to introduce the intensity disturbance in the laser modes (just before the beam profiler).

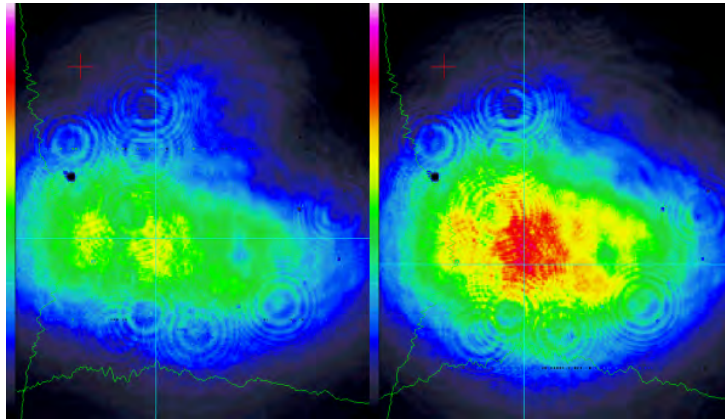


Figure 4.2: Mode filtered trough steel pinhole, with and without metal fibre.

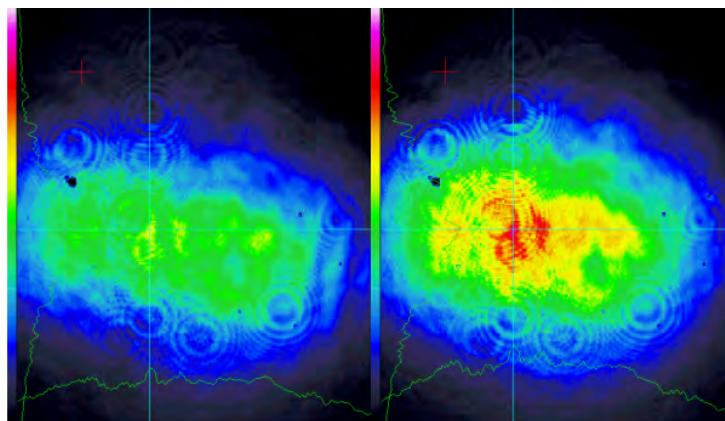


Figure 4.3: Mode filtered trough glass pinhole, with and without metal fibre.

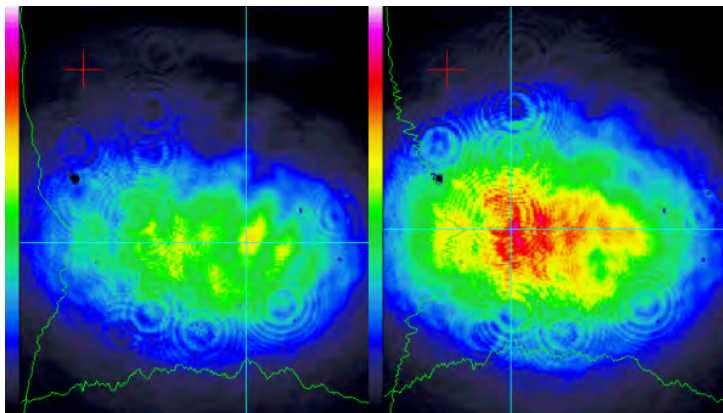


Figure 4.4: Mode filtered trough glass with small α pinhole, with and without metal fibre.

4.1.1 Future work on spatial filtering

When a new pinhole is inserted into the spatial filter it has to be aligned to the beam. For a conical pinhole both the position of the exit and its tilt have to be adjusted. The alignment of the pinhole position is done with the help of two apertures before and after the spatial filter (A_{23}) and the XY translator, which the pinhole is mounted on. When conventional pinholes are used, which is easy to exchange and not very expensive, this alignment procedure is no problem. But for conical pinhole, where the alignment is crucial, if no laser induced damage is to occur, this alignment procedure might be a problem. It would be preferable to have some sort of detection system to see if the alignment is correct. This is important for the adjustments of the tilt of the pinhole as well, so that no reflected light is collected. Today there is no possibility to see if intensity modulations in the near field are introduced by the pinhole due to a tilt.

If a camera, detecting the near field after mirror M_4 were installed the information received would help to align the pinhole. A fine adjustment of the pinhole position (relative to the beam) could be done with mirror M_1 (manually controlling the mirror with help of the program used for the automatic alignment). In this case a very fast and precise alignment of the pinhole would be possible together with the possibility to constantly monitor the filtered mode. A camera placed after M_4 could be used to align the laser beam relative to the third optical table as well at the same time.

Today the alignment of the spatial filter is performed manually (before the automatic alignment is turned on) with two apertures (A_2 and A_3 in

figure 1.2.

In the present setup a lens with $f = 1.5\text{ m}$ is used giving a spot size of $300\text{ }\mu\text{m}$ (FWHM). Due to problems with plasma formation, a lens with longer f would be preferable. A larger spot size means a larger pinhole and decreased intensity at its surface. Problems in manufacturing the pinhole would also decrease. The manual alignment of the pinhole would be more precise and easier to perform. If the spatial filter lenses are exchanged there are some issues that should be considered. When the $f_{\#}$ (focal length/beam diameter) of the lenses is increased the effect of pulse front delay is reduced, however this reduction is small. If the pulse length in the system is reduced in the future the effect of this will be more prominent and it should perhaps be considered using achromatic doublets instead or mirrors to focus the beam in the spatial filter.

When amplifying crystals are used close to their damage threshold, the absence of spatial noise in the beam is important. In this system the beam is passed through the second multi-pass amplifier (4 round trips) after the spatial filter. When amplification/pump energy is increased the crystal will be very sensitive for hot-spots. Especially sensitive in the last round trip when the fluence is high and there is a possibility that high spatial frequencies have been built up during the previous three passes. If it is possible to install a second spatial filter before this last pass it might be possible to increase amplification even further.

4.2 Automatic alignment

The automatic alignment system developed in the present project is today operating routinely and correcting the beam direction through the first multi-pass amplifier and the spatial filter of the high power laser. The alignment system has been proven to work well and is a robust system.

A log of focal point position in the spatial filter (when the automatic alignment system is in operation) can be seen in figure 4.5. The improvement is clear when this is compared with the systems behaviour without automatic alignment illustrated in figure 3.1.

4.2.1 Future work on automatic alignment

The automatic alignment system is today correcting the beam direction through the spatial filter with only one controllable mirror and the error detection is performed with a single camera. It is possible to upgrade the

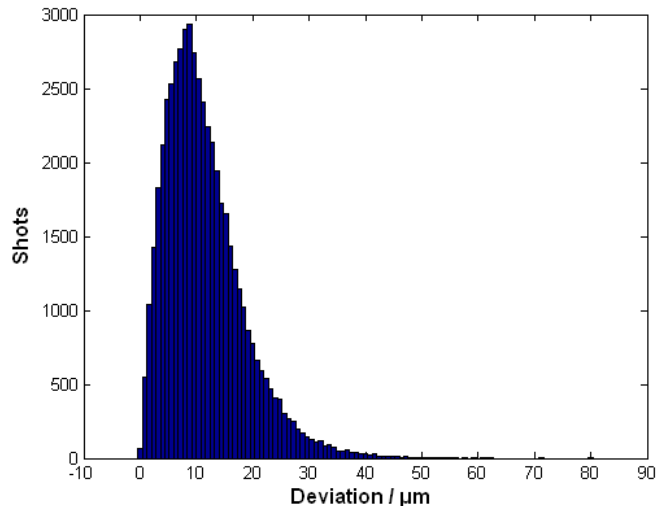


Figure 4.5: Histogram of total error of the focal point position during 13h operation.

alignment system in the future to be able to control more than one mirror and therefore be able to handle a more complete alignment of the laser.

In the part of the laser system after the spatial filter (third optical table in figure 1.2) there are also some problems with misalignment occurring during a day of operation. These should be possible to reduce with an improved alignment system. One of the main factors that causes problems in this part is that the present alignment system is fixing the beam direction relative to optical table number 2 where the spatial filter is mounted. After the spatial filter the beam is directed to optical table number 3. During the day these two tables move slightly relative to each other, causing a drift on the third table. How large the drift is and if it changes behaviour (if the beam position or its direction changes, or both) during the day has not yet been measured.

Some proposals on different possible improvements are presented in the sections below.

Proposal to further improve the automatic alignment system

The easiest improvement would be to add a second system, controlling the beam direction into the last multi-pass amplifier. The advantage is that this would be simple, in principle two separated systems. There are however some problems concerned with this solution. The last amplifier is often operated in single shot mode and this would prevent the camera, which would have

to be placed after the shutter, to receive any signal between these shots. Because both creeping¹ of the piezoelectric crystals and the fact that the system requires several shots to align the beam would be a problem. There are, however, ways to handle this problem, and two such ideas are presented below.

It should be possible to use a separate, continuous wave, alignment laser. The alignment beam has to be injected into the beam path at the same optical table as the spatial filter is attached. Otherwise it will not be possible to align the laser at the optical table number 3. A possible advantage with this method is that it would be possible to use a faster sampling speed than 10 Hz and therefore be able to compensate for faster disturbances than in the alignment system used today.

Another solution could be to add a second shutter after the amplifier preventing unwanted shots to pass to the experimental area. The shutter used today could then allow enough shots to pass before the "single shot" for the alignment system to be able to align the laser. The second shutter would then work as a beam block during alignment, i.e. one "button" for aligning the system and one to fire the single-shot. This solution is very simple and no extra optical components would be needed. A disadvantage might be that about 2 seconds of alignment shots has to be passed before each shot in single-shot mode.

As positive side effect of an automatic alignment of the second multi-pass amplifier would be that the focus drift in the experimentation area would also decrease.

The part of the laser system after the spatial filter is presently not protected from air turbulence in any way which causes a shot-to-shot variation in the experimental area. Perhaps it should be considered to do some improvements on optical table number 3 similar to the box confining optical table 2. The alignment performed by an automatic alignment system would be better if the shot-to-shot variations were small.

A more complete alignment through the amplifying crystals

An improved alignment would be reached if two mirrors were controlled before each multi-pass amplifier. Both the direction and position of the beam could in this case be controlled. This should improve amplification and reduce astigmatism. This requires an extra camera for each amplifier and a more complicated control algorithm.

¹Creeping occurs in piezoelectric material and causes the crystal to change size without any change in applied voltage.

It is possible to install two cameras for each multi-pass amplifier, one placed before the amplifier and the other placed after and two controllable mirrors placed before the amplifier. The first controlling the beam position and the second controlling the direction of the beam through the amplifier. This would give an almost perfectly aligned beam entering the amplifier.

Chapter 5

Conclusions

The automatic alignment system built for the Lund Terawatt Laser System to align the spatial filter and one of the multi-pass power amplifiers has proven to be a robust system that works well. To use a personal computer together with LabView, a digital camera and an internal D/A card to deliver a control signal has been a good choice. The specially designed piezoelectric controlled mirror mount works well and the stroke length of the crystals is enough for compensating for the daily drift in the system. However, saturated control signals are quite common and an additional stroke length of the piezoelectric crystals would prevent such cases. And since the entire alignment system works as well as it does and the precision in the control signal delivered to the piezo-driven mount exceed expectations the limited stroke length in the crystals is somewhat annoying. If a similar system were to be built it would be preferable to use piezoelectric actuators (built for the purpose) with long stroke length instead of the specially designed mirror mount and the original equipment manufacturer (OEM) piezoelectric crystal used today.

When high threshold pinholes of glass were first suggested during this project the aim was to let 500 mJ pulses pass the spatial filter without plasma formation at the pinhole. Tests with borosilicate pinholes ($f = 1.5$ m and $d_{exit} = 0.6$ mm) with flat exit surface show problems with plasma formation for 500 mJ pulse energies but not for 130 mJ. Pinholes with an angle $\beta < 90$ degrees have not yet been tried in long term use to determine if they will handle those high intensities. However pinholes of stainless steel can still be used and with the new alignment system the lifetime should be enough even with 500 mJ passing through the spatial filter.

Chapter 6

Acknowledgements

I would like to thank my supervisor Claes-Göran Wahlström for all the inspiration and ideas, and most of all for giving me the confidence and letting me work at the Lund terawatt laser. A great thanks to Anders Persson who has helped me with most of the practical work on the laser system.

I would also like to thank Olle Lundh and Filip Lindau for all their help, and Lars Rippe for helping me out with my first steps in LabView programming, which made this project possible. I would further like to thank the Applied Molecular Spectroscopy group for letting me use some of their equipment and, of course others at the Atomic Physics department who have helped me but are not mentioned above.

Bibliography

- [1] O. Svelto. *Principles of Lasers*. Plenum Press, 4th Ed., 1998.
 - [2] F.L. Pedrotti, S.J. and L.S. Pedrotti. *Introduction to Optics*. Prentice Hall International, 2nd Ed., 1996.
 - [3] J. O. Cormier X. Zhu and M. Piche. Study of dispersion compensation in femtosecond lasers. *Journal of Modern Optics* **43**, 8, 1996.
 - [4] Zsolt Bor. Femtosecond-resolution pulse-front distortion measurements by time-of-flight interferometry. *Optics Letters* **14**, 16, 1989.
 - [5] S. A. Letzring N. A. Kurnit and R. P. Johnson. A high-damage-threshold pinhole for glass fusion laser applications. *SPIE* **3492**, pages 896–900, 1999.
 - [6] G. Korn J. Squier D. Du, X. Liu and G. Mourou. Laser-induced breakdown by impact ionization in SiO_2 with pulse widths from 7ns to 150fs. *Applied Physics Letters* **64**, 23, 1994.
 - [7] Z. Liu H. Chen T. Q. Jia, R. X. Li and Z. Z. Xu. Threshold of ultra-short pulse laser-induced damage in dielectric materials. *Applied Surface Science* **189**, 333, 2002.
 - [8] D. von der Linde and H. Schuler. Breakdown threshold and plasma formation in femtosecond laser-solid interaction. *J. Opt. Soc. Am. B* **13**, 1996.
 - [9] A.E. Chmel. Fatigue laser-induced damage in transparent materials. *Materials Science and Engineering*, pages 175–190, 1997.
 - [10] A. Morono P. Martin and E. R. Hodgson. Laser induced damage enhancement due to stainless steel deposition on ks-4v and kul quartz glasses. *Journal of Nuclear Materials*, 2004.
-

-
- [11] J. Hermann T. Itina M. Sentis, Ph. Delaporte and O.Uteza. Laser micro-machining applications developed. http://www.ncla.ie/apps_ultrafast_apps.htm, 2004.
- [12] F. Bonneau and P. Combis. Theoretical modeling of lase interaction in spatial filter pinholes for high energy pulsed lasers. *SPIE* **3578**, pages 250–255.
- [13] R. J. Wallace J. E. Murray L. B. Da Silva B. J. MacGowan B. M. Van Wonterghem P. M. Celliers, K. G. Estabrook and K. R. Manes. Spatial filter pinhole for high-energy pulsed lasers. *Applied Optics* **37**, 12, 1998.
- [14] J. T. Hunt J. M. Auerbach, N. C. Holmes and G. J. Linford. Closure phenomena in pinholes irradiated by nd laser pulses. *Applied Optics* **18**, 1979.
- [15] C. Kittel. *Introduction to solid state physics*. John Wiley sons, inc. seventh edition, 1996.
- [16] <http://www.americanpiezo.com>.
-

Appendix A

The Beam Control program

The Beam Control program is written in LabView (National Instruments). It is a sequential program where the loop is executed each time an image is received from the camera. The program consists of several virtual instruments (VI), which are described below. All VI:s will be described as they are run, from beginning to end.

A.1 Main VI, 'Beam Control.vi'

First the settings are read from the file 'settings.ini'. See Figure A.1. The camera is initialised from the cluster 'Camera Settings'. See Figure A.2. At the same time values to several constants and variables are set. See Figure A.3.

All images that will be needed in the program are created, 'Raw Image', 'Threshold', 'Showed Image' and 'Saved Image'.

The image from the camera is stored in 'Raw Image' which is then sent to the subVI 'Center.vi' where the estimation of the focal spot coordinates is done. 'Raw Image' is also sent to the subVI:s 'hair cross.vi' (where a hair cross is overlaid) and 'save image.vi' (where the image saved to disk).

When the center coordinate has been estimated the values (x- and y- coordinates) are sent to subVI 'control.vi' together with the desired coordinates from the cluster 'Center Settings'. See Figure A.4.

The control signals are further sent to a subVI to update the channels of the D/A card and to the subVI 'Block.vi' to determine if any of the control signals are saturated and to block the beam if necessary. See Figure A.5 and A.6.

The desired and actual coordinates of the focal point position are sent to the two case structures in figure A.7 where new coordinates can be chosen

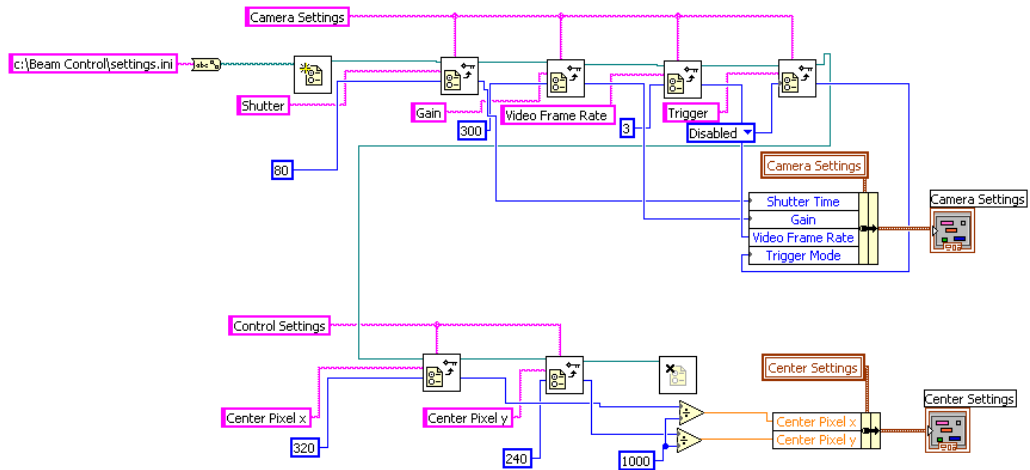


Figure A.1: Camera settings and the desired focal spot coordinates on the CCD chip are read from 'settings.ini'. The values from the file are stored in two clusters, 'Center Settings' and 'Camera Settings'. The values read from 'settings.ini' are divided by 100 before stored in 'Center Settings'. The reason is that when the standard VIs for configuration files are used the data after the decimal points are not used. Therefore when pixel coordinates are stored in 'settings.ini' they are multiplied by 100.

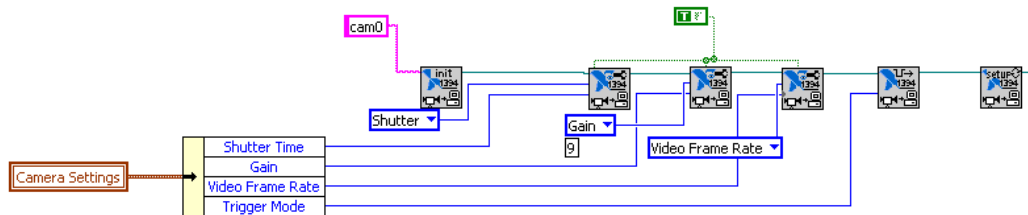


Figure A.2: The cluster 'Camera Settings' is initialising the camera. The camera name 'cam0' is given by the LabViews Measurement & Automation to label the camera.

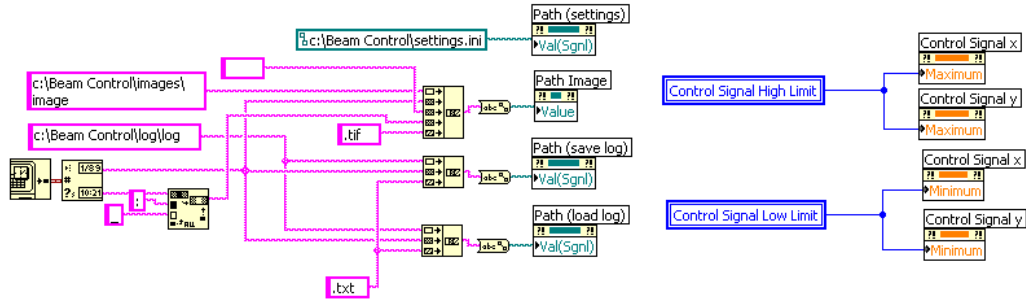


Figure A.3: Default pathes and limits of control signals

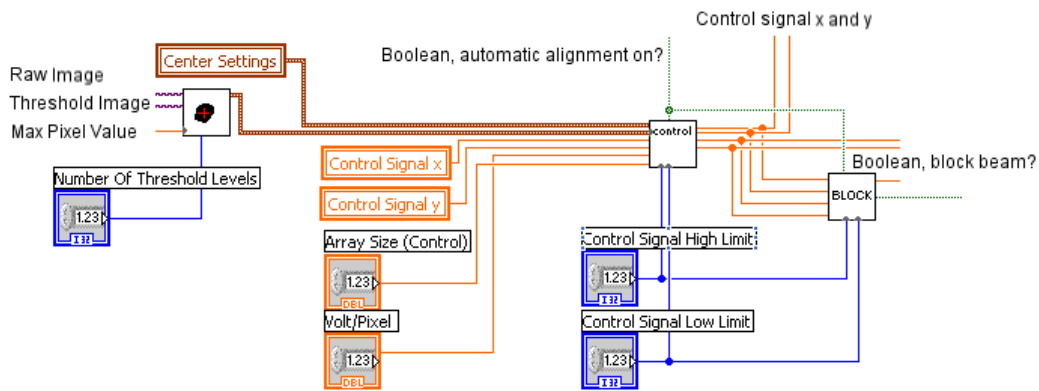


Figure A.4: Calculation of control signals

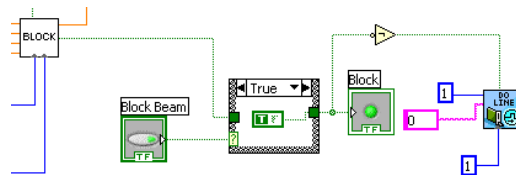


Figure A.5: A Boolean variable is sent to subVI 'PLV Write to Digital Line.vi' to update the digital line used to control a beam shutter.

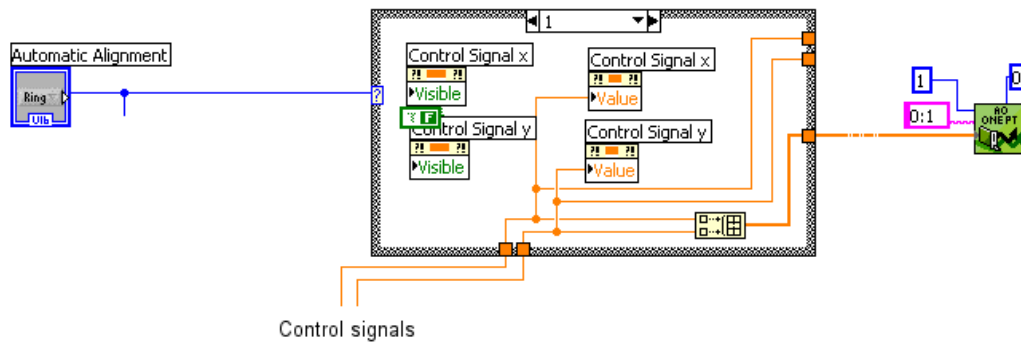


Figure A.6: Control signal is sent to the subVI 'DAQ-LVIEW AO Update Channels.vi' to update the analogue channels if automatic alignment is chosen in the ring 'Automatic Alignment'.

and stored in cluster 'Center Settings' or the desired saved in 'settings.ini'.

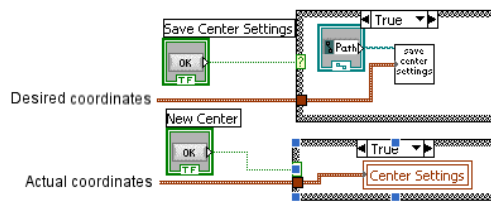


Figure A.7: New coordinates are stored in the cluster 'Center Settings'. Desired coordinates are stored in 'settings.ini'.

A log is by default saved when the program is used. By default data for every 10:th shot is saved, defined by the integer 'Interval' (value 1 means every shot). With the ring 'Delimiter' it is possible to chose ',' or '.' as decimal point. See Figure A.8

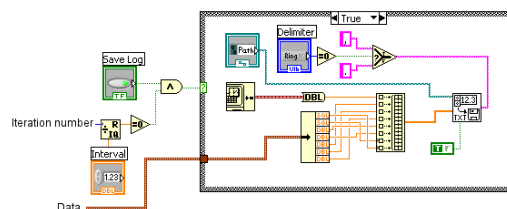


Figure A.8: Save log

The saved data for each shot are from right to left in the log text file: time (LabView standard time: second since 12:00 a.m., January 1, 1904), error x (pixels), error y (pixels), total error (pixels), control signal x (V), control signal y (V), max pixel value and mean pixel value.

A.1.1 SubVI:s

'Center.vi'

In this VI the center coordinates of the focal point are estimated. The 'Raw Image' is thresholded and saved in 'Threshold Image'. The number of threshold levels is chosen with the integer 'Number of Threshold Levels'. The first threshold level is chosen as the maximal pixel value in 'Raw Image' divided by the variable 'First Threshold Level'. The other threshold levels are equally dividing $2/3$ of the remaining "foot" from the first threshold level of the image. Then a mean value is estimated from the different threshold levels to get the actual coordinates stored in the cluster 'Actual Centroid'. See Figure A.9.

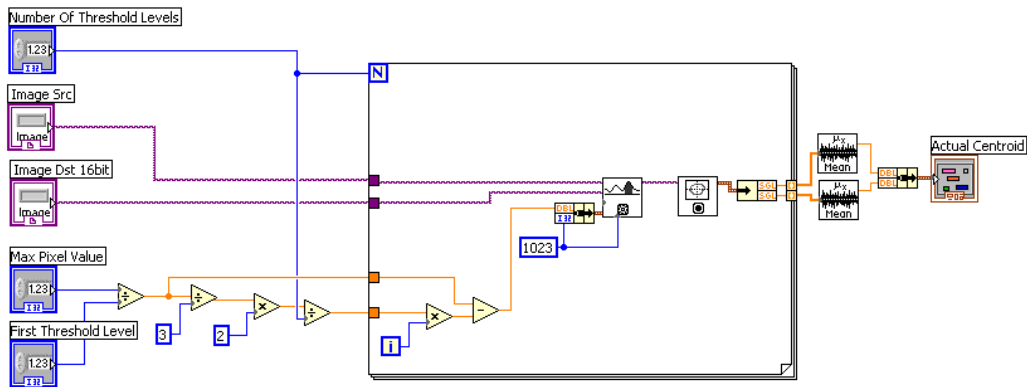


Figure A.9: Estimation of center coordinates

'Control.vi'

In 'control.vi' the control signal is estimated as

$$S_n = C \cdot \text{error} + S_{n-1}$$

where C is a constant, S_n is the new control signal and S_{n-1} is the control signal from the previous loop.

An error is estimated from the two clusters 'Actual Centroid' and 'Desired Centroid'. To suppress fast variation in the focal point position a median value, over the latest errors (specified by 'Array size') stored in 'Array x' and 'Array y', is estimated. The error is multiplied by a constant ('Volt/Pixel'), which is added to the control signal from the previous loop. See Figure A.10.

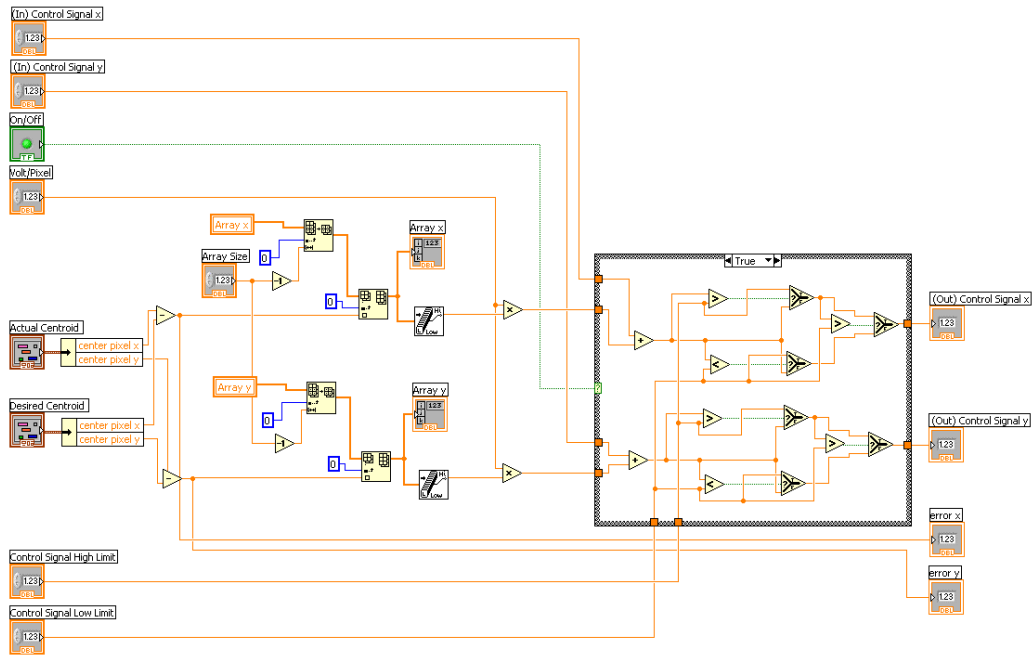


Figure A.10: Estimation of control signals

The case structure is used to turn off the automatic alignment to a manual control of the control signals. Inside the case structure seen in figure A.10 the control signals are saturated at the values defined by 'Control Signal High Limit' and 'Control Signal Low Limit'.

'Block.vi'

This VI is used to send a TTL signal to a physical beam shutter. The shutter is opened if the automatic alignment is on and none of the control signals is saturated. The errors of the latest 10 shots are compared to the variable 'Limit'. This is done in the array 'Array Error'. If any of the errors has exceeded the limit at all these shots and the control signals has been saturated the beam is blocked. See Figure A.11.

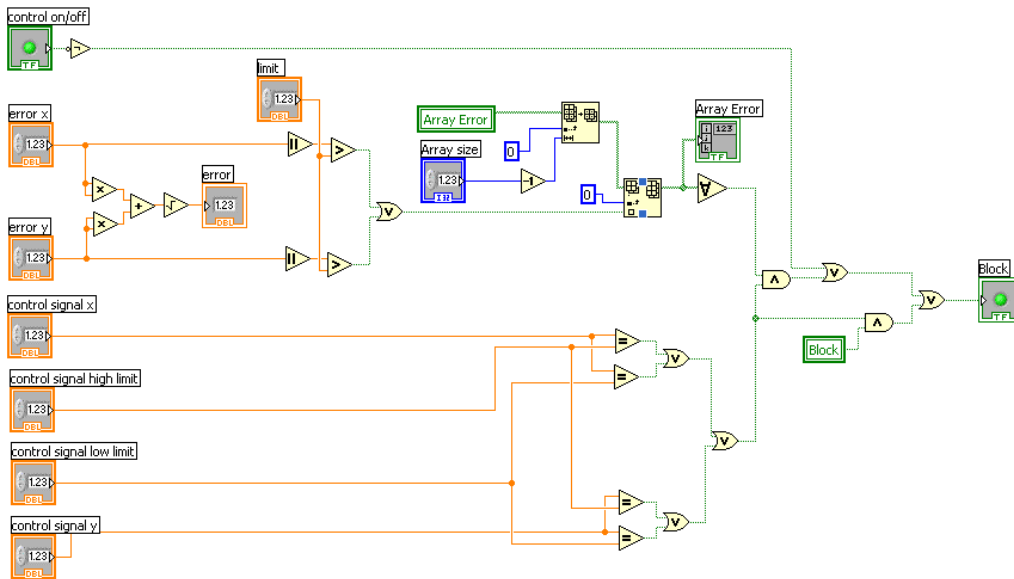


Figure A.11: 'Block.vi' that determines if any of the control signals are saturated.

'DAQ-LVIEW AO Update Channels.vi' and 'PLV Write to Digital Line.vi'

These VI:s have been supplied by the manufacturer of the D/A card (Adlink Technology inc.). The desired output signals is simply wired to the VI:s with the specified channels. See Figure A.12. Which channel associated with which pin on the physical card is shown in figure A.13. In this case pin 19, 37 and 23 are used (V0, V1 and DO0).

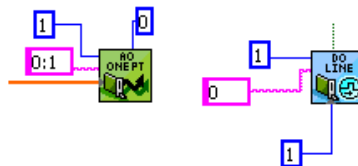


Figure A.12: Update analogue and digital channels on the D/A card

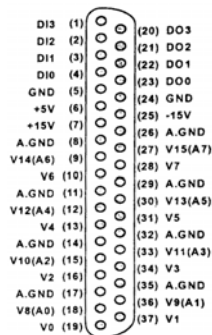


Figure A.13: Connector pin assignment on D/A card. The analogue output pin are specified as V_n and A_n (Voltage and Current). The digital input and output pin are specified as DI_n DO_n .

'Hair cross.vi'

In subVI 'hair cross.vi' two lines (forming a hair cross) and one circle is overlaid on the image 'Raw Image'. The sizes of the overlaid structures are defined by constants inside the VI.

'Write To txt File.vi'

The standard VI 'Write To txt File.vi' has been modified to be able to store the time with high enough precision and the possibility to use both ',' and '.' as decimal points.

A.1.2 Other VIs

'PCI-6208V Analog Output.vi'

The VI 'PCI-6208V Analog Output.vi' is used to update all analogue channels of the D/A card.

'Load Log.vi'

The VI 'Load Log.vi' is used to load and view previously recorded logs.

Appendix B

Camera

IEEE-1394 digital camera

- ✓ 6 Pin IEEE-1394 interface
- ✓ External trigger
- ✓ Automatic inter-camera synchronization
- ✓ Computer controlled camera parameters
- ✓ Image acquisition software
- ✓ CS mount or micro-lenses





The Dragonfly is a fully digital video camera that conforms to the DCAM 1.30 and the "IEEE 1394 standards". The Dragonfly uses a 1/3" progressive scan CCD in order to stream VGA quality images at 30 FPS without compression. The camera is provided as a complete system with an IEEE 1394 interface card, cable, and image acquisition software.

The Dragonfly is an OEM-style IEEE-1394 board level camera specifically designed for industrial machine vision tasks. The Dragonfly was created to provide maximum control and flexibility for digital imaging applications. Through the IEEE-1394 interface, the computer communicates digitally with the camera, allowing reliable transmission of images and software control of camera parameters.

Network capable
An IEEE-1394 hub can be used to connect multiple Dragonfly cameras on the same bus. By connecting the hub to a PC host it is possible to simultaneously acquire images from any one of the cameras. Four B&W Dragonfly cameras can simultaneously broadcast at 640x480 resolution at 30 frames per second (FPS) and seven cameras can broadcast at 15FPS. Three cameras can simultaneously broadcast at 1024x768 resolution at 15 FPS.

Camera synchronization
When more than one Dragonfly camera is present on the IEEE-1394 bus, the cameras automatically synchronize their acquisition time to within 120µs. This feature is particularly important in applications where an image of an object needs to be acquired from multiple points of view at exactly the same time. Please contact us if you require a large number of synchronized cameras.

External trigger
The Dragonfly camera has an external trigger feature that provides control over timing of the image acquisition. The external trigger feature is defined by the IEEE-1394 based Digital Camera Specification (ver 1.30). This is used in applications where the image acquisition has to be synchronized with an outside event.



dragonfly

Firmware upgrading
The Dragonfly allows users to upgrade its firmware through the IEEE-1394 interface. Our upgrade software allows camera features to be easily upgraded in-field. For example, extended exposure time was a feature added to the camera after it started shipping. Please visit our web page frequently for updates of camera features or contact us with your specific needs.

Peripheral control
The Dragonfly has four I/O pins that can be configured in one of four ways. The pins can be set up for external trigger, CCD integration strobe output, digital input and output. This feature is useful for integrating the camera with external devices such as process controllers and lighting lights.

Camera parameter control
Host software provided with the Dragonfly camera allows manual and automatic control of the camera parameters, such as the CCD integration time and the gain. In the color version, the software allows control of white balance.




www.ptgrey.com

Point Grey Research (PGR) is a worldwide leader in the development of advanced digital camera technology products. Based in Vancouver, British Columbia, PGR designs, manufactures and distributes IEEE-1394 cameras, stereo vision cameras and spherical digital video cameras to a broad spectrum of industries. Through a close working relationship with its customers, PGR continues to be at the forefront of innovation.

IEEE-1394 digital camera

Camera Specifications:

Imaging Device:	1/3" Sony CCD 640x480 Option: ICX084, B&W or Color 1024x768 Option: ICX204, B&W or Color HAD image sensor with square pixels Progressive scan All models available with an extended CCD head
Supported frame rates:	640x480 Option: 30, 15, 7.5, 3.75 FPS 1024x768 Option: 15, 7.5, 3.75, 1.875 FPS
Supported formats:	B&W models: 8-bit or 16-bit Mono Color models: 8-bit or 16-bit Bayer tiled image (color space conversion done on the host computer)
Digital camera specification:	Version 1.30
Signal to noise ratio:	Greater than 60dB
Connector:	6-pin IEEE-1394
Power:	Through IEEE-1394, less than 2.0W
Shutter:	Auto/Manual (1/30s to 1/8000s @ 30Hz at 640x480; 1/15s to 1/6000s @ 15Hz at 1024x768). Shutter time can be extended up to 60 seconds.
Gain:	Auto/Manual (640x480: 0 - 30dB, 0.035dB resolution) (1024x768: 0 - 27dB, 0.035dB resolution)
Synchronization:	Less than 120µs
External Trigger:	DCAM 1.30 Trigger Mode 0, see diagram
Lens focal length:	4, 6 and 8mm focal length, M12 micro-lenses (12mm diameter, 0.5mm pitch) C/S mount lens holders available
Footprint:	2.5" X 2" see diagram



Package includes:

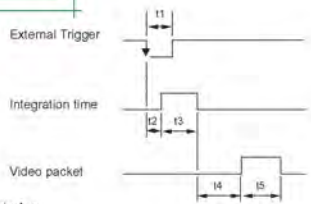
- ✓ Dragonfly camera
- ✓ 4.5 meter, 6-pin, IEEE-1394 cable
- ✓ IEEE-1394 OHCI PCI Interface card
- ✓ 4, 6 and 8mm focal length M12 micro lenses
- ✓ CS mount lens holder
- ✓ Tripod mounting bracket
- ✓ Dragonfly camera driver
- ✓ Image acquisitions software

System requirements:

- ✓ Intel Pentium II or better
- ✓ Windows 2000 or XP

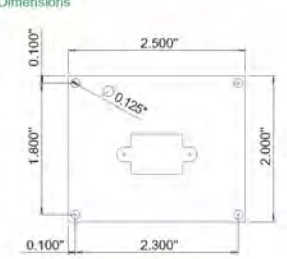
External Trigger

The Dragonfly camera implements the External Trigger feature as specified in the IEEE-1394 Digital Camera Specification Version 1.30.




t1: min 1µs
t2: less than 63µs
t3: integration time
t4: 1 ms
t5: 30 ms (240 packets) (Mode_5, 30fps)

Dimensions



subscribe to our
electronic newsletter

please email newsletter@ptgrey.com



305-1847 West Broadway, Vancouver, B.C., Canada V6J 1Y6
T: 604-730-9937 F: 604-732-8231 www.ptgrey.com

Continuing product development is vital to Point Grey Research. Point Grey Research reserves the right to alter any published specifications without notice.